Mon. Not. R. Astron. Soc. **330,** 17–34 (2002)

μJy radio sources in the $z = 0.83$ cluster MS1054−03

P. N. Best,[1]★ P. G. van Dokkum,[2]† M. Franx[3] and H. J. A. Röttgering[3]

[1]*Institute for Astronomy, Royal Observatory Edinburgh, Blackford Hill, Edinburgh EH9 3HJ*
[2]*California Institute of Technology, Mail Stop 105-24, 1200 E. California Blvd, Pasadena, CA 91125, USA*
[3]*Sterrewacht Leiden, Postbus 9513, 2300RA Leiden, the Netherlands*

Accepted 2001 September 25. Received 2001 September 3; in original form 2001 January 17

ABSTRACT

An extremely deep 5-GHz radio observation is presented of the rich cluster MS1054−03 at redshift $z = 0.83$. 34 radio sources are detected down to a 6σ level of 32 μJy, compared with about 25 expected from previous blank-field radio source count determinations; the sources giving rise to these excess counts lie predominantly within 2 arcmin (∼700 kpc) of the cluster centre. Existing imaging and spectroscopic observations have provided optical identifications for 21 of the radio sources and redshifts for 11, of which eight are confirmed cluster members. Four of these eight confirmed cluster sources are associated with close galaxy pairs (10–25 kpc projected offset) of similar magnitude, implying that the radio source may be triggered by an interaction. However, although MS1054−03 has a very high fraction (17 per cent) of ongoing mergers (separations $\ll 10$ kpc), no radio emission is detected towards any of these merger events, setting a mean upper limit of $10\,M_{\odot}\,yr^{-1}$ for any star-formation associated with these mergers. This supports the hypothesis that low-luminosity radio sources may be onset by initial weak interactions rather than direct mergers. The host galaxies of the other four confirmed cluster radio sources are all isolated, and show a range of morphologies from early type to Sc. A comparison between the emission-line and radio luminosities suggests that two of these four radio sources are low-luminosity active galactic nuclei (AGNs), whilst for at least one of the other two the radio emission is associated with ongoing star formation. All the radio sources associated with the galaxy pairs appear more likely to be AGN than starburst in origin. The overall proportion of radio sources associated with AGNs in this cluster (≳75 per cent) is higher than that detected at these flux-density levels in the field (40–50 per cent).

Key words: galaxies: clusters: individual: MS1054−03 – galaxies: evolution – galaxies: starburst – radio continuum: galaxies.

1 INTRODUCTION

Clusters of galaxies are the largest, most massive, collapsed structures in the Universe and, although only a small fraction (≈5 per cent; Dressler 1984) of all low-redshift galaxies lie in cluster environments, clusters play a key role in studies of galaxy evolution since they contain large numbers of galaxies at the same distance. The central regions of clusters are dominated by a population of luminous early-type galaxies which occupy a narrow locus in colour–magnitude relations and show a tight relationship between their effective radius, effective surface brightness, and central velocity dispersion (the fundamental plane, Dressler et al. 1987; Djorgovski & Davies 1987); these relations evolve with redshift out to $z = 0.83$ roughly in accordance with passive evolution predictions, with no significant increase in scatter (e.g. Schade, Barrientos & Lopez-Cruz 1997; van Dokkum et al. 1998a,b; Stanford, Eisenhardt & Dickinson 1998). However, Butcher & Oemler (1978) showed that by redshift $z \sim 0.3$ a substantial population of bluer galaxies appears in many, but not all, clusters. These bluer galaxies are almost all disc galaxies, of which many exhibit strong Hα or [O II] 3727-Å emission lines indicative of recent star formation (e.g. Dressler et al. 1997, 1999). These results point strongly to a higher level of activity in high-redshift clusters.

In addition to star-formation activity, galaxies can also display nuclear activity associated with an active galactic nucleus (AGN). One of the cleanest methods of searching for either of these forms of activity is to utilize the radio emission. AGN are extremely luminous at radio wavelengths, with luminosities reaching as high as about 10^{28} W Hz^{-1} at 1.4 GHz. Normal (i.e. non-AGN) galaxies have a range of observed radio luminosities, between about 10^{18}

★E-mail: pnb@roe.ac.uk
†Hubble Fellow

and $10^{24}\,\mathrm{W\,Hz^{-1}}$ at 1.4 GHz, with starbursting galaxies filling the upper half of that range. The radio emission arising from these normal galaxies comes predominantly from the synchrotron emission of particles accelerated in supernova shocks (e.g. Condon 1992 and references therein), with a smaller thermal contribution from H II regions, and so essentially reflects the current star formation of the galaxy.

At redshifts $z \gtrsim 0.2$ the radio luminosities of luminous starburst galaxies and weak AGNs correspond to microjansky flux-density levels, and over recent years numerous μJy-level radio surveys of the field have been carried out (Fomalont et al. 1991; Windhorst et al. 1993; Donelly, Partridge & Windhorst 1997; Richards 1998; Muxlow 1999; Garrett 2000). The integral radio source count shows an upturn below a couple of mJy, indicating the emergence of a new population of radio sources at microjansky levels (Windhorst, van Heerde & Katgert 1984; Windhorst et al. 1985); indeed, a large proportion of the μJy radio source population has been shown to be associated with starburst galaxies and normal spiral galaxies at substantial redshifts $z \gg 0.2$ (e.g. Windhorst et al. 1995). The steep slope of the differential source counts of μJy radio sources, similar to that of the very powerful radio galaxies and quasars, implies that this population of sources, if it is a single population, is undergoing strong cosmological evolution with either the density or luminosity of the sources being higher in the past. This is in broad agreement with determinations of the evolution of the cosmic star-formation rate (Madau, Pozzetti & Dickinson 1998), suggesting that studies of μJy radio sources are important for understanding the star-formation history and evolution of ordinary galaxies (Haarsma et al. 2001).

Whilst deep μJy field surveys have made considerable progress in recent years, no studies of radio sources in distant clusters have been carried out to comparable depth. At low redshift ($z < 0.09$), the radio luminosity function in clusters, when viewed in terms of the proportion of optical galaxies that have a given radio luminosity, is statistically indistinguishable from that of the field (Ledlow & Owen 1996). This is somewhat unexpected since the onset of a starburst or AGN is likely to be induced either by an infall of gas onto the galaxy or through a weak interaction or merger with a companion galaxy: it would be natural to assume that each of these phenomena would occur at a different rate in cluster environments than in the field. In low-redshift clusters, the similarity may be due to the relatively relaxed states of the clusters, with much of the gas and galaxies lying in stable virialized orbits and the gas having been stripped from the galaxies in the cluster centre (e.g. Gunn & Gott 1972): these effects reduce interactions and prevent a higher fraction of radio sources forming in these environments. Clusters of galaxies at higher redshifts, however, may still be in their formation process, with relatively high galaxy merger rates (e.g. van Dokkum et al. 1999) and a plentiful supply of disturbed gas. These should provide ideal laboratories to induce starbursts and AGN (cf. the high fraction of post-starburst galaxies in $z \sim 0.5$ clusters; Poggianti et al. 2000).

Dwarakanath & Owen (1999) carried out a detailed radio study of two $z \approx 0.25$ clusters, Abell 2125 and Abell 2645, which have similar redshifts and richnesses (Abell class 4), but very different fractions of Butcher–Oemler blue galaxies; Abell 2125 has a blue galaxy fraction of 0.19, whereas that of Abell 2645 is only 0.03. They found that the radio luminosity distribution of cluster members of Abell 2125 is bimodal, with a peak at about $10^{24.5}\,\mathrm{W\,Hz^{-1}}$ composed entirely of AGNs, and a second higher peak at or below (owing to the detection limit) $10^{22.5}\,\mathrm{W\,Hz^{-1}}$ composed of a mixture of AGNs and star-forming galaxies (see Section 5.4 for more details). In Abell 2645, many fewer radio sources were detected, with essentially the entire lower luminosity class of sources missing. The presence of this lower luminosity class of radio sources therefore seems to be connected with the presence of the blue Butcher–Oemler galaxies, although the two populations do not overlap strongly: only one of the blue galaxies in the Abell 2125 cluster has an associated radio source.

Smail et al. (1999) have made a deep radio observation (rms $1.4 \times 10^{22}\,\mathrm{W\,Hz^{-1}}$ in our assumed cosmology) of the $z = 0.41$ cluster CL0939+4713 and detect eight cluster radio sources,[1] associated with a range of galaxy morphologies from ellipticals through to Sd-type galaxies. At higher redshifts, Stocke et al. (1999) have studied radio galaxies in clusters with redshifts $0.3 < z \lesssim 0.8$ to a limiting point source 1.4 GHz radio luminosity of $10^{23.5}\,\mathrm{W\,Hz^{-1}}$. They found no evidence for evolution of the population of radio sources between redshift $z \sim 0.8$ and the present epoch. However, their observations are only sensitive enough to detect the brighter of the two populations of cluster radio sources discovered by Dwarakanath & Owen (1999), and it is the fainter population that appears to depend upon the dynamical state of the cluster, and hence may be expected to show strong redshift evolution.

The goal of the current project, therefore, is to investigate in detail the nature of the fainter radio source population in high-redshift clusters. This aim was addressed by carrying out a deep VLA observation of the rich cluster MS1054−03 at $z = 0.83$. The nature of this cluster and the existing observations of it are described in Section 2, and the new VLA observations are described in Section 3. The radio source population is investigated and compared with the optical imaging data in Section 4. In Section 5 an analysis is made of the cluster radio source population, including a detailed comparison of the radio, optical and emission-line properties of the cluster galaxies. Conclusions are drawn in Section 6. Throughout the paper, cosmological parameters of $\Omega = 1$, $\Lambda = 0$ and $H_0 = 70\,\mathrm{km\,s^{-1}\,Mpc^{-1}}$ are assumed.

2 THE $z = 0.83$ CLUSTER MS1054−03

With a redshift of $z = 0.83$, MS1054−03 is the highest redshift cluster in the Extended Medium Sensitivity Survey (EMSS) X-ray-selected cluster sample (Gioia et al. 1990), and also one of the most luminous in X-rays with a 0.3–3.5 keV X-ray luminosity of $9 \times 10^{44}\,\mathrm{erg\,s^{-1}}$. On account of its high redshift and richness (Abell class 3), a deep 5 by 5-arcmin mosaic was made of the field around the cluster using the wide-field planetary camera 2 (WFPC2) on the Hubble Space Telescope (*HST*), in two filters (F606W and F814W; van Dokkum et al. 2000). This has subsequently been supplemented by deep near-infrared imaging of the cluster in the *J*-, *H*- and *K*-bands using the NTT, and *U*, *B*, *V* imaging using FORS on the VLT, to provide galaxy colours across a long wavelength baseline (Franx et al., in preparation). These images show a conspicuous overdensity of red cluster galaxies with a somewhat irregular and elongated distribution (van Dokkum et al. 2000), probably consisting of three sub-clumps of galaxies at the same radial velocity; this is consistent with the detection of substructure in the X-ray image (Donahue et al. 1998; Jeltema et al. 2001).

[1] Here the blended entries labelled 296 and 230 by Smail et al. are taken to be part of the same extended radio source, since even if separated into two sources the far brighter 296 entry still remains resolved.

Multi-object spectroscopy carried out on the Keck Telescope has enabled redshifts to be determined for over 200 objects in this field, with more than 130 of these being confirmed as cluster members (van Dokkum et al. 2000; Tran et al., in preparation). These authors found that the fraction of all early-type galaxies in the central regions of the cluster is 46 per cent, much lower than that at low redshift (∼80 per cent). Further, a very high fraction (17 per cent) of cluster galaxies are classified as 'merger/peculiar' on the basis of double nuclei (separations $\leqslant$10 kpc), tidal tails, and distorted morphologies (van Dokkum et al. 1999). This high fraction strongly argues against monolithic collapse models of galaxy formation. Interestingly, many of the merging galaxies are red, bulge-dominated galaxies with no detected nebular line emission, and colours offset from the early-type $(U-B)_z$ colour magnitude relation by only 0.07 mag. The fraction of blue galaxies in the cluster, calculated in a manner equivalent to that defined by Butcher & Oemler (1978), is 0.22 ± 0.05 (van Dokkum et al. 2000), comparable with the mean value determined for clusters at redshifts $0.3 < z < 0.5$.

MS1054−03 is clearly an interesting rich cluster with a wealth of observations over a wide variety of wavelengths and, crucially, with spectroscopic redshifts for the majority of the objects towards the cluster centre: currently, spectroscopic redshifts have been measured for 80 per cent of all galaxies with $19.0 < I < 22.0$ (the brightest cluster galaxy has $I \sim 19.5$) within the bounds of the *HST* mosaic. As such, MS1054−03 is an ideal target for a deep cluster radio survey. Indeed, it was one of the high-redshift clusters in the 1.4 GHz survey of Stocke et al. (1999), who detected three radio sources within the cluster down to a flux-density limit of 0.2 mJy. These are discussed later, together with the weaker sources identified in the current observations.

3 OBSERVATIONS AND DATA REDUCTION

3.1 Observations and calibration

MS1054−03 was observed using the Very Large Array (VLA) at 5 GHz in C array configuration during three 10-hour runs on 2000 April 3, 6 and 7. The total on-source integration time was 96 270 s. The observations were carried out simultaneously at two frequencies, 4835 and 4885 MHz, each with two circular polarizations and 50-MHz bandwidth. With this set-up, the full-width-half-power of the antenna primary beam is about 9 arcmin and the angular resolution about 4 arcsec.

The observations were carried out using standard VLA procedures. Short observations of the primary flux calibrator 3C 286 (1331+305) were used to calibrate the flux-density scale, assuming flux densities of 7.46 and 7.51 Jy at the two observing frequencies; these are the most-recently determined VLA values, and are approximately 1 per cent above the flux-density scale of Baars et al. (1977). Observations of 3C 286 separated in time by about 6 h were used to determine the absolute polarization position angle and to estimate the uncertainty in this calibration ($\pm 2°$) from the difference between the solutions for the two different scans. The secondary calibrator 1058+015, offset 5 degrees from MS1054−03, was observed at 30-minute intervals throughout the runs to provide accurate phase calibration. The wide range of parallactic angles at which this calibrator was observed enabled the on-axis antenna polarization response terms to be determined accurately.

3.2 Editing and imaging

After first discarding data from any antenna or baseline showing excessive noise (very little for the first run, about 5 per cent of the data from the second run and 10 per cent of the data from the third run), the data were CLEANed using the AIPS task IMAGR. Then, the presence of a just-sufficiently bright (7 mJy) point source towards the centre of the field enabled two cycles of phase self-calibration to be carried out, which reduced the map rms by 10–15 per cent. Final maps of the field were then produced in the Stokes parameters I, Q and U by further CLEANing the data sets. The maps were produced using an intermediate data weighting between those of natural and uniform weighting, by setting the data weighting ROBUST parameter to 0.5. This weighting provided the best compromise between the higher sensitivity of a naturally-weighted map and the higher angular resolution of a uniformly-weighted map: the rms noise level was only eight per cent higher than that of natural weighting, and a Gaussian restoring beam of full-width-half-maximum (FWHM) 5 arcsec (north–south) by 4.5 arcsec (east–west) was used. A second total intensity map was also made at full angular resolution (4.0 by 3.9 arcsec FWHM) using uniform weighting to allow more detailed investigation of the source structural parameters; the rms noise level was about 70 per cent higher than that of the ROBUST = 0.5 map.

Maps of the field of size 1024×1024 pixels, with pixel size 1.0 arcsec were made. Extra CLEAN boxes were placed around a further six sources outside this field, to prevent any increase in the map noise due to their sidelobes, but these extra sources are not considered further in this paper since they are well beyond the primary beam for these observations and are unlikely to be associated with the cluster. 25 000 CLEAN iterations were used, which CLEANed the maps down to a level of 2.0σ. Although negative CLEAN components were found after a much smaller number of iterations, this deep CLEANing is essential to remove the source sidelobes fully. A contour plot of the Stokes I 5-by-4.5-arcsec resolution map of the field is displayed in Fig. 1.

3.3 Source extraction and properties

The resultant rms noise of the lower-resolution maps is 5.3 ± 0.1 μJy, within a few per cent of the theoretically expected value, indicating the success of the editing and calibration procedures. Real sources were taken to be those that had either a peak image flux density[2] in excess of 32 μJy (6σ), or a peak flux density in excess of 21 μJy (4σ) and extended structure whose integrated image flux density was detected above the 6σ level. There are no negative regions that would be selected according to these criteria if the sign of the radio flux density were inverted across the entire map, and so it is reasonable to expect that all the extracted sources are real. Only those sources within 400 arcsec of the pointing centre (corresponding to 80 per cent primary-beam attenuation) were considered. 34 sources were thus selected from the image, and are detailed in Table 1.

The absolute position of each source was determined, together with its position relative to the cluster centre (as determined by the

[2] Note that due to primary beam attenuation the true sky flux densities are higher than the observed image flux densities at large radii; see discussion of corrections later in this section. For clarity, in this paper the term 'sky flux density' is adopted for the true flux density of the source and the term 'image flux density' refers to the (uncorrected) lower value measured on the images due to primary beam attenuation.

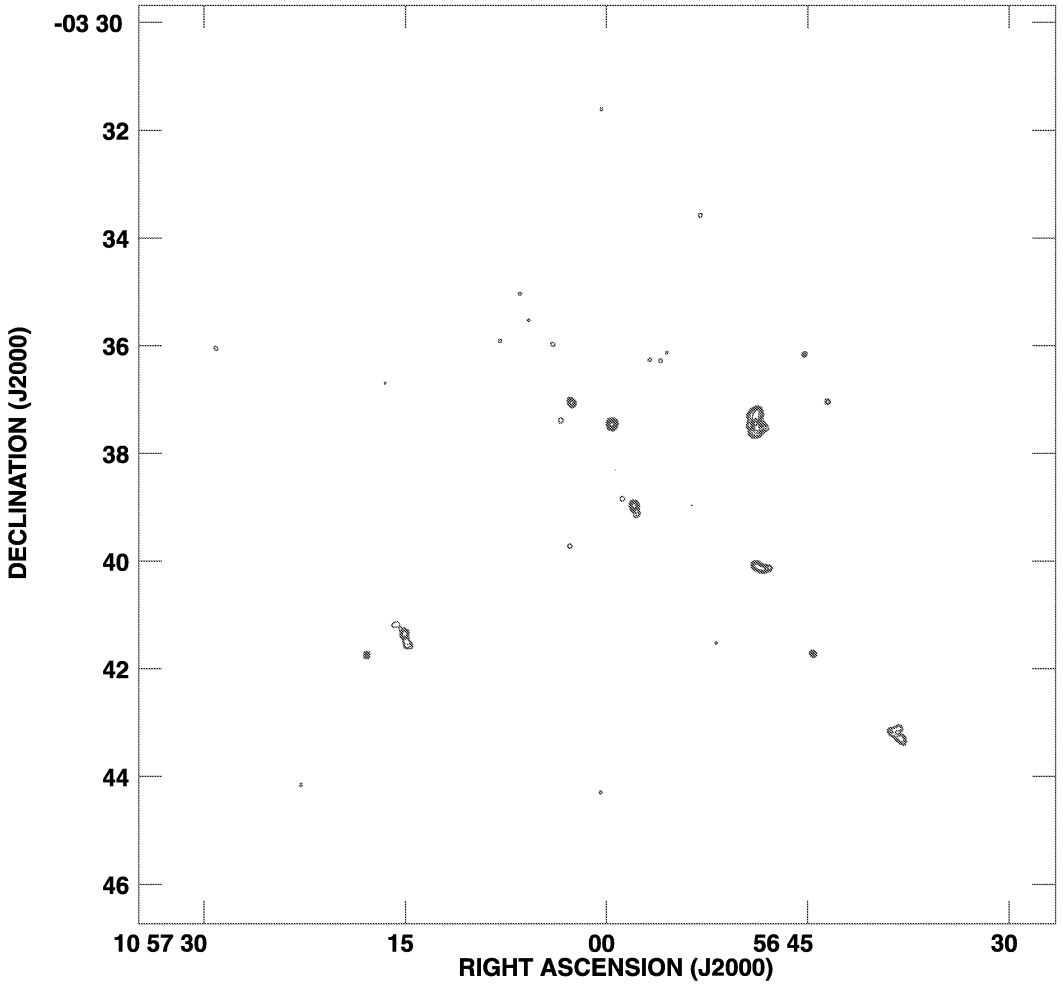

Figure 1. The contour map of the 1024-by-1024-arcsec field around the centre of the cluster MS1054−03. The image rms noise level is 5.3 μJy beam^{-1}, and contours are plotted at $(-2, -1, 1, 2, 4, 8, 16, 32, 64, 128, 256, 512) \times 32$ μJy beam^{-1} (6σ), though note that owing to primary beam attenuation (for which this map has not been corrected) the true sky flux densities are somewhat higher at large angular separations from the pointing centre: the antennae primary beam FWHP is about 9 arcmin.

optically-selected brightest-cluster galaxy). For extended sources, note that the quoted position is the position of the peak of the radio flux, and may not accurately correspond to the location of the associated optical galaxy. Similarly for the very faintest sources the theoretically determined errors may be somewhat optimistic.

The peak flux density of each source was measured directly from the image, and corrected for the effects of chromatic aberration: the 50-MHz bandwidth leads to radial smearing of a true point source, and results in the measured peak flux density being decreased by 5 per cent at 230 arcsec radius, and 10 per cent at 345 arcsec radius for these observations. For unresolved or barely-resolved sources, the integrated flux density was calculated from a Gaussian fit using the AIPS task JFMIT. Sources that are clearly extended, or of such low signal-to-noise ratio that Gaussian fitting may be misleading, had their integrated flux density calculated by summing the flux density within a small box placed around the source. No correction has been made for surface brightness biases (e.g. Pascarelle, Lanzetta & Fernández-Soto 1998), which should be fairly negligible at the relatively-low angular resolution of these observations. The image flux densities were then corrected for primary beam attenuation to determine the true sky flux density of each source. This attenuation is approximately 50 per cent at a radius of 270 arcsec. For those sources that were either extended or resolved, the integrated flux density was taken and corrected to determine the true sky flux density; for the unresolved sources, the peak flux density was used. All three flux densities are provided for each source in Table 1.

Morphological parameters of each source were determined using JFMIT: for sources brighter than 60 μJy, the higher-angular-resolution uniformly-weighted map was used for this, with the lower-resolution higher-sensitivity map being used for the weaker sources. The deconvolved angular size of each source was determined, or an upper limit set thereon, after correction for radial smearing due to the non-zero bandwidth. Each source was classified as either: (i) unresolved (U), if only an upper limit could be set to its angular size; (ii) possibly resolved (R/U) if an angular size was determined but the one-sigma lower limit was below zero; (iii) resolved (R), if the source was clearly resolved; or (iv) extended (E), if the intensity distribution could not be fitted using a single Gaussian profile. In the later case, some indication of the nature of the radio source is also provided in the table. It should be noted here that no attempt has been made to correct for any overestimation of the angular sizes that may occur due to the presence of noise when fitting small radio sources detected at only

Table 1. The radio properties of the radio sources in the field. Provided are: (1) the source catalogue name, ordered in increasing distance from the centre of the cluster; (2,3) the right ascension and declination of the source; (4) the offset in arcsec of the radio source from the centre of the cluster, as defined by the position of the optically-brightest cluster galaxy, which is at 10 57 00.02, −3 37 36.0 (J2000); (5,6) the peak and integrated image flux densities of the radio source (see text); (7) the sky flux density of the source after correction for primary beam attenuation; (8) where the redshift of the source is known (see Table 3), the rest-frame 5-GHz radio luminosity of the source, assuming a spectral index of 0.8; (9) the nature of the source (U – unresolved; R/U – possibly resolved; R – resolved; E – extended); (10) the angular size of the source; (11) the position angle of the source.

Source	RA (J2000)	Dec. (J2000)	Δr [arcsec]	S_p [μJy]	S_{int} [μJy]	S_{corr} [μJy]	$\log(L_{5\,GHz})$ [W Hz^{-1}]	Nature	Θ [arcsec]	PA [deg]
(1)	(2)	(3)	(4)	(5)	(6)	(7)	(8)	(9)	(10)	(11)
MS1054−C1	10 56 59.59 ±0.00	−3 37 27.7 ±0.0	10.6	7302.0 ±5.3	7309.0 ±10.7	7302.0 ±5.3	25.1	U	<0.5	—
MS1054−C2	10 57 02.03 ±0.05	−3 37 31.4 ±0.7	29.9	21.3 ±5.3	33.2 ±8.9	32.1 ±8.9	22.7	R/U	4.8 <7.9	54
MS1054−C3	10 57 02.60 ±0.01	−3 37 03.6 ±0.1	50.5	341.0 ±5.3	461.0 ±12.6	465.7 ±12.7	23.9	R	3.5 ±0.2	36
MS1054−C4	10 57 03.41 ±0.06	−3 37 23.6 ±0.7	53.0	51.9 ±5.3	228.0 ±24.0	230.5 ±24.1	—	E [Diffuse]	≈15	140
MS1054−C5	10 57 03.80 ±0.05	−3 37 42.7 ±0.4	57.0	24.2 ±5.3	38.2 ±8.4	38.8 ±8.5	22.8	R/U	4.3 <6.9	75
MS1054−C6	10 57 04.09 ±0.03	−3 37 07.8 ±0.4	67.0	35.3 ±5.3	51.5 ±7.1	52.8 ±7.3	23.0	R/U	3.2 <5.1	108
MS1054−C7	10 56 58.86 ±0.02	−3 38 51.4 ±0.2	77.4	61.1 ±5.3	91.6 ±7.2	95.0 ±7.5	—	R/U	1.5 <2.3	41
MS1054−C8	10 56 57.93 ±0.01	−3 38 58.0 ±0.1	87.9	839.0 ±5.3	1358.0 ±22.6	1428.0 ±24.1	24.4	E [Core-jet]	≈8	148
MS1054−C9	10 56 56.86 ±0.02	−3 36 16.0 ±0.2	92.9	60.9 ±5.3	61.1 ±6.4	64.5 ±6.3	—	U	<3.2	—
MS1054−C10	10 56 55.97 ±0.01	−3 36 16.7 ±0.2	99.8	52.3 ±5.3	47.6 ±8.0	56.1 ±6.3	—	U	<2.8	—
MS1054−C11	10 56 55.51 ±0.02	−3 36 08.4 ±0.3	110.6	40.5 ±5.3	39.8 ±7.3	44.3 ±6.4	—	U	<2.7	—
MS1054−C12	10 57 03.99 ±0.01	−3 35 58.9 ±0.2	114.5	63.4 ±5.3	63.7 ±6.8	69.7 ±6.5	23.1	U	<2.5	—
MS1054−C13	10 56 53.70 ±0.02	−3 38 58.0 ±0.3	125.2	40.6 ±5.3	39.4 ±6.7	45.8 ±6.7	—	U	<3.5	—
MS1054−C14	10 57 02.73 ±0.02	−3 39 43.2 ±0.3	133.5	56.0 ±5.3	62.2 ±8.3	71.7 ±9.6	23.1	U	<4.3	—
MS1054−C15	10 57 00.01 ±0.03	−3 35 13.5 ±0.5	142.5	28.5 ±5.3	72.3 ±14.2	85.3 ±16.7	22.1	R	7.2 ±1.5	168
MS1054−C16	10 57 05.85 ±0.02	−3 35 32.4 ±0.3	151.3	38.9 ±5.3	37.9 ±7.2	47.1 ±7.1	—	U	<3.1	—
MS1054−C17	10 57 07.95 ±0.02	−3 35 54.8 ±0.3	156.0	47.4 ±5.3	45.3 ±7.0	58.2 ±7.2	—	U	<3.2	—
MS1054−C18	10 56 48.90 ±0.01	−3 37 26.9 ±0.1	166.7	1029.0 ±5.3	6023.0 ±36.0	7653.0 ±93.5	23.8	E [FR I]	≈22	7
MS1054−C19	10 57 06.46 ±0.02	−3 35 02.2 ±0.2	181.5	49.7 ±5.3	63.7 ±8.5	85.3 ±11.5	—	R/U	2.7 <4.0	125
MS1054−C20	10 56 48.59 ±0.01	−3 40 07.2 ±0.1	228.3	485.3 ±5.3	1493.0 ±23.6	2396.5 ±58.9	—	E [FR I?]	≈11	69
MS1054−C21	10 56 45.25 ±0.02	−3 36 09.8 ±0.2	237.3	69.2 ±5.3	77.6 ±8.3	130.4 ±14.0	22.6	U	<3.8	—
MS1054−C22	10 56 43.53 ±0.01	−3 37 02.6 ±0.1	249.0	106.0 ±5.3	104.5 ±6.1	188.3 ±10.5	—	U	<1.6	—
MS1054−C23	10 57 16.50 ±0.03	−3 36 41.7 ±0.4	252.6	39.4 ±5.3	49.9 ±7.5	90.1 ±13.7	—	U	<4.3	—
MS1054−C24	10 57 16.53 ±0.03	−3 38 45.1 ±0.4	256.6	33.8 ±5.3	38.1 ±7.6	70.2 ±14.0	—	U	<4.6	—
MS1054−C25	10 56 53.02 ±0.02	−3 33 34.6 ±0.3	263.2	56.6 ±5.3	58.7 ±5.9	107.4 ±10.1	—	U	<3.6	—
MS1054−C26	10 56 51.88 ±0.02	−3 41 31.4 ±0.4	265.1	39.9 ±5.3	41.8 ±6.2	76.4 ±10.1	—	U	<3.8	—
MS1054−C27	10 56 50.23 ±0.04	−3 33 42.9 ±0.6	275.4	29.6 ±5.3	71.4 ±9.7	143.9 ±19.6	—	R	6.3 ±2.4	70
MS1054−C28	10 56 46.09 ±0.03	−3 41 32.7 ±0.4	315.4	32.0 ±5.3	30.8 ±5.6	79.9 ±13.3	—	U	<3.2	—
MS1054−C29	10 56 39.37 ±0.03	−3 38 49.3 ±0.6	317.7	30.0 ±5.3	41.9 ±7.9	106.3 ±20.0	—	R/U	4.1 <5.7	23
MS1054−C30	10 57 15.07 ±0.01	−3 41 21.2 ±0.1	318.6	550.7 ±5.3	1230.8 ±32.1	3131.8 ±124.8	—	E [FR I (II?)]	≈28	11
MS1054−C31	10 56 44.61 ±0.01	−3 41 43.3 ±0.1	338.2	167.6 ±5.3	168.3 ±6.1	484.4 ±23.4	—	U	<2.5	—
MS1054−C32	10 57 00.36 ±0.02	−3 31 36.0 ±0.3	360.1	45.2 ±5.3	47.3 ±6.2	153.2 ±18.0	—	U	<3.2	—
MS1054−C33	10 57 17.88 ±0.01	−3 41 44.9 ±0.1	365.3	166.2 ±5.3	174.0 ±9.4	589.4 ±30.3	—	U	<3.0	—
MS1054−C34	10 57 23.00 ±0.60	−3 35 15.0 ±5.0	371.8	26.8 ±5.3	424.0 ±56.0	1600.0 ±200.0	—	E [Diffuse]	≈60	110

the few-sigma level (e.g. Windhorst et al. 1984). This effect is negligible for the brighter sources, but could be $\gtrsim$10 per cent for the weakest sources: as a guide, the angular sizes of the fainter sources in the sample are typically about 15 per cent higher if determined from the 5 arcsec resolution image than from the 4 arcsec resolution image used.

4 THE μJY RADIO SOURCE POPULATION

4.1 Comparison with background counts

Numerous field surveys have been carried out of the μJy radio source population to determine the differential radio source counts at different radio frequencies (see the introduction). Fomalont et al. (1991) have derived a parametrization for the integral source count at 5 GHz of: $N(>S) = (23.2 \pm 2.8)S^{-1.18\pm0.19}$, where $N(>S)$ is the number of sources per square arcmin with a total flux density greater than S, measured in μJy. This formula can be used to predict the mean number of background sources that is expected in a 400 arcsec radius circle reaching a flux-density limit of 32 μJy at the centre, taking into account the variation in the sensitivity with radius due to primary beam attenuation. That gives a background prediction of about 25 ($\pm$5) sources which, compared with the 34 sources observed, suggests that of order a quarter of the detected sources are likely to be associated with the cluster.

This analysis can be taken a step further by investigating the radial distribution of radio source counts in the cluster. In Fig. 2 the number of detected sources is compared with the expected number of background sources as a function of distance from the centre of the cluster. A clear (>99 per cent significant) excess of sources is detected in the inner 2 arcmin radius, corresponding to about 700 kpc at the redshift of the cluster. Beyond this radius, the number counts of detected sources are fully consistent with background predictions. These results are also provided numerically in a number of radial annuli in Table 2.

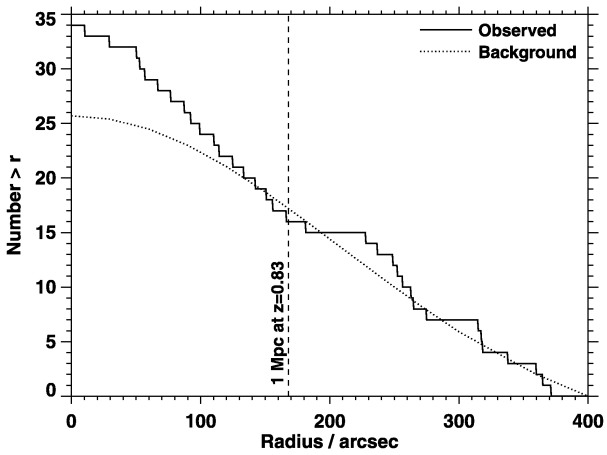

Figure 2. The cumulative distributions (working from a radius of 400 arcsec into the centre of the cluster) of detected radio sources (solid line) compared with the predicted background counts (dotted line). The observed distribution is fully compatible with expectations at large radii, but a clear excess of sources, significant at the >99 per cent significance level, is detected at small radii. These excess counts correspond to the radio sources associated with the cluster, and are found within a radial distance of order 700 kpc (evaluated at $z = 0.83$).

Table 2. The distribution of radio sources with distance from the cluster centre, compared with the expected background counts. For each radius range (1) the table provides the mean radius (2), the limiting sky flux density at that radius (3) (this corresponds to a limiting image flux density of 32 μJy corrected for the primary beam attenuation factor), the mean number of background sources per square arcmin expected above this flux density (4), the total number of background sources expected to be detected in this radius range, together with the expected variation assuming Poisson statistics (5), and the true number of sources detected (6). A clear excess of detected sources is seen in the inner 2 arcmins, which corresponds to about 700 kpc at the redshift of the cluster (see also Fig. 3).

Radius [arcsec]	$\bar{R}$ [arcsec]	$\bar{S}_{\rm lim}$ [μJy]	$N(>S_{\rm lim})$ [arcmin^{-2}]	$N_{\rm bk}$	$N_{\rm obs}$
(1)	(2)	(3)	(4)	(5)	(6)
0–60	42	32.0	0.389	1.2 ± 1.1	5
60–120	95	33.9	0.363	3.4 ± 1.8	7
120–180	153	38.7	0.310	4.9 ± 2.2	6
180–240	212	48.0	0.241	5.3 ± 2.3	3
240–300	272	63.0	0.175	4.9 ± 2.2	6
300–360	331	87.7	0.118	4.1 ± 2.0	4
360–400	381	129.1	0.075	2.0 ± 1.4	3

4.2 Radio–optical comparisons: the optical data

As discussed in Section 2, an *HST* WFPC2 mosaic of the MS1054−03 cluster has been made covering an area of 5 by 5 arcmin for an exposure time of 6500 second per pointing per filter in each of the F606W (R) and F814W (I) filters. This reaches a depth in the I-band of $I \sim 26$ for a point source. VLT observations using FORS in the U-, B- and V-bands have also been taken, covering a sky area of 6.8 by 6.8 arcmins and reaching a point source limiting depth (3σ) in the V-band of $V \sim 27$ (Franx et al., in preparation).

To compare the radio and optical data, the two data sets must be placed in the same astrometric frames. Radio observations are automatically in the International Celestial Reference Frame (ICRF), with positional errors significantly below 0.1 arcsec, but the absolute positions of optical images can be uncertain at the arcsec level. Initial astrometry of the optical frames was taken from the *HST* astrometric headers, after correction for geometric distortions (van Dokkum et al. 2000). This astrometry was then improved by considering the relative radio and optical positions of those unresolved radio sources that had unambiguous optical counterparts and adjusting the optical astrometry to produce the minimum combined radio–optical offsets for these sources, taking into account the uncertainties on the optical and radio positions of each source. This improvement resulted in a small offset of the optical frames by 0.17 arcsec E and 0.13 arcsec N from the astrometry of van Dokkum et al., with the central cluster galaxy now having a position of 10 57 00.02, −3 37 36.0 (J2000). The resultant optical frame astrometry should be within 0.2 arcsec of the ICRF. The magnitudes and positions of the optical galaxies were obtained using SExtractor (Bertin & Arnouts 1996) on the *HST* image mosaic (van Dokkum et al. 2000).

4.3 Radio–optical correlations

The location of each radio source relative to the centre of the cluster is given in Table 3, together with details of any optical galaxies with $I < 26$, that lie within 2.5 arcsec of the radio source.

Table 3. Comparisons between the radio sources and the optical data. For each source, the offset (in arcsec) of the radio source from the central cluster galaxy (at 10 57 00.02, −3 37 36.0, J2000) in RA (positive is West) and Dec. (positive is North) is given. For those sources that lie within the fields of the optical imaging, details of any optical galaxy brighter than $I = 26$ within 2.5 arcsec of the radio position are also given. The old identification numbers of each galaxy are taken from the original numbering scheme for the *HST* imaging observations (van Dokkum et al. 2000), with a value of −99 indicating a galaxy previously without a number. The new identification numbers represent a reclassification including all galaxies on the *HST* frame, introduced for the spectroscopic observations: these new identification numbers will be used in all forthcoming papers. The offsets δx and δy are from the central cluster galaxy, as defined for the radio sources, and the 'Offset' column gives the positional difference (in arcsec) between the radio and optical locations. The morphological type of the galaxy is given where known, as is its magnitude through the F814W ($\sim I$) filter of the *HST* and the F606W − F814W($\sim R - I$) colour for those objects within the *HST* mosaic. The penultimate column gives the source redshift, if measured, and the final column indicates with 'C' the confirmed cluster galaxies, and with 'P' the potential galaxy pairs.

Source	Radio source		Optical galaxies within 2.5 arcsec									
	δx	δy	Old id.	New id.	δx	δy	Offset	Type	F814W	F606W−F814W	z	Note
MS1054−C1	6.4	8.3	1459	4705	6.1	8.3	0.3	Sc	20.66	1.71	0.8452	C
MS1054−C2	−30.1	4.6	1435	5442	−29.7	4.5	0.4	S0/a	21.87	1.96	0.8195	CP
			1431	5432	−29.4	2.3	2.4	Sa/b	22.11	1.59	0.8148	CP
			1433	5465	−32.3	5.7	2.5	–	22.63	1.91	1.0760	
MS1054−C3	−38.6	32.4	1656	5529	−37.8	31.2	1.4	E/S0	21.06	2.09	0.8216	CP
			1655	5534	−37.9	34.1	1.9	E	20.94	1.86	0.8397	CP
MS1054−C4	−50.7	12.4	–	–	–	–	–	–	–	–	–	
MS1054−C5	−56.6	−6.7	1403	5599	−56.8	−5.5	1.2	Sc	20.14	1.31	0.8113	C
MS1054−C6	−61.0	28.2	1584	6038	−61.5	28.3	0.5	E	20.76	2.13	0.8311	CP
			−99	6143	−59.4	27.2	1.9	–	23.49	0.55	–	
			−99	6164	−63.2	28.3	2.2	E	21.49	2.11	–	P
			−99	6145	−59.6	30.2	2.5	–	22.80	0.65	–	
MS1054−C7	17.4	−75.4	735	4362	17.4	−74.9	0.5	–	21.82	0.88	–	
MS1054−C8	31.2	−82.0	−99	4012	31.0	−82.8	0.8	S0/a	21.50	1.98	0.8297	CP
			710	3995	30.5	−81.0	1.2	E	20.78	2.14	0.8342	CP
MS1054−C9	47.3	80.0	1865	3456	49.5	79.0	2.4	Star	17.82	1.85	–	
MS1054−C10	60.6	79.3	1851	3104	60.8	78.9	0.4	–	23.53	0.78	–	
			1851	3070	60.0	79.6	0.6	–	23.44	1.07	–	
MS1054−C11	67.5	87.6	1895	2847	67.8	87.7	0.3	–	23.30	0.71	–	
			−99	2825	67.9	85.2	2.5	–	24.62	0.56	–	
MS1054−C12	−59.4	97.9	1942	5756	−59.3	97.9	0.1	E	20.98	2.09	0.8309	C
MS1054−C13	94.6	−82.0	−99	2036	94.1	−82.2	0.5	Sa/b	21.92	1.63	–	
			−99	1943	96.3	−80.2	2.5	–	23.87	0.76	–	
MS1054−C14	−40.6	−127.2	−99	564	−41.1	−127.5	0.6	–	–	–	0.8321	C
MS1054−C15	0.1	142.5	2132	4416	−0.6	142.9	0.7	Sc	17.96	1.23	0.2499	
MS1054−C16	−87.3	123.6	–	–	–	–	–	–	–	–	–	
MS1054−C17	−118.7	101.2	−99	7702	−118.3	101.7	0.6	–	25.91	–	–	
MS1054−C18	166.5	9.1	1592	1	166.6	9.7	0.6	E	16.54	0.85	0.1830	
MS1054−C19	−96.4	153.8	2151	–	−95.9	154.0	0.5	–	–	–	–	
MS1054−C20	171.1	−151.2	519	–	171.2	−152.8	1.6	–	–	–	–	
MS1054−C21	221.1	86.2	−99	8	221.6	85.4	0.9	E/S0	18.56	1.21	0.3740	
MS1054−C22	246.8	33.4	−99	–	246.7	32.7	0.7	–	–	–	–	
MS1054−C23	−246.7	54.3		---Outside optical fields---								
MS1054−C24	−247.1	−69.1		---Outside optical fields---								
MS1054−C25	104.8	241.4	–	–	–	–	–	–	–	–	–	
MS1054−C26	121.9	−235.4		---Outside optical fields---								
MS1054−C27	146.6	233.1	−99	–	147.4	232.2	1.2	–	–	–	–	
MS1054−C28	208.5	−236.7		---Outside optical fields---								
MS1054−C29	309.1	−73.3	−99	–	308.7	−73.1	0.5	–	–	–	–	
MS1054−C30	−225.3	−225.2		---Outside optical fields---								
MS1054−C31	230.7	−247.3		---Outside optical fields---								
MS1054−C32	−5.1	360.0		---Outside optical fields---								
MS1054−C33	−267.4	−248.9		---Outside optical fields---								
MS1054−C34	−344.0	141.0		---Outside optical fields---								

If multiple optical candidates are found, only those within 3 mag of the brightest galaxy are listed, to minimize potential galaxy deblending problems. The 2.5 arcsec radius considered is larger than the 0.2 arcsec uncertainty in the astrometric frame discussed above, primarily due to uncertainties in both the radio and optical positions.

Contour plots of the 34 radio sources are displayed in Fig. A1 in the appendix, overlaid where possible upon an optical image of the field. The nature of each individual source is also discussed there. From these results it is seen that of the 34 radio sources, 25 lie within the fields of the optical imaging. All but four (MS1054−C4, C9, C16, C25) of these sources have optical counterparts that are very probably associated with the radio source. 10 radio sources are associated with optical galaxies with magnitudes typical of the bright cluster galaxies ($19 \lesssim I \lesssim 22$), and a further 11 associated with galaxies whose magnitudes are either unmeasured or fall outside of this range. It should be noted that although towards the very centre of the cluster the sky density of detected sources is high, with of order 200 galaxies with $I \lesssim 26$ detected in the centre-most square arcmin (1 galaxy per 18 square arcsec), in this region all the radio–optical coincidences are with bright optical galaxies ($I < 22$). At these magnitudes the probability of an optical galaxy

being at the observed radio–optical offsets is very low (≪5 per cent; from $P(<r) = 1 - \exp(-\pi\rho r^2)$, where ρ is the sky density of optical sources); however, even in the cluster outskirts the probability of chance coincidence with an optical galaxy of $I \sim 25$ is as high as ∼25 per cent. It should also not be forgotten that any true radio source hosts with $I > 26$ may lie within 2.5 arcsec of a brighter galaxy, and so be misidentified.

5 THE CLUSTER RADIO SOURCE POPULATION

Of the 21 sources with optical identifications, spectroscopic redshifts are available for 11 of the host galaxies, and eight (assuming here that MS1054−C2 is associated with one or both of the cluster galaxies; see the appendix) of these lie at the redshift of the cluster. This section concentrates upon these eight cluster radio sources. Fig. 3 provides a detailed picture of the radio–optical correlations and optical morphologies of these galaxies.

It should be noted that although only eight of the 34 radio sources are confirmed to be associated with the cluster, these eight galaxies are likely to comprise the majority of the cluster radio population brighter than 32 μJy: the confirmed cluster galaxies stand out from the background population not only through the excess radio source counts and their location in the inner 700 kpc radius from the cluster centre, but also by their association with galaxies of magnitudes $20 < I < 22$ and red ($R - I \gg 1$) colours (see Table 3); only two of the radio sources without redshifts (MS1054 − C7 and C13) are associated with galaxies with measured magnitudes in this range, of which only C13 is red. Therefore conclusions based upon the properties of these eight can be interpreted more generally.

An approximate comparison between the radio luminosities and star-formation rates of (non-AGN) cluster galaxies can be made by converting between the type II supernova rate and the radio emission, since star-forming regions are transparent at radio wavelengths: $L_\nu \approx 1.3 \times 10^{23} \nu^{-\alpha} n_{\rm SN}\,{\rm W\,Hz^{-1}}$, where ν is measured in GHz, $\alpha \simeq 0.8$ is the radio spectral index and $n_{\rm SN}$ is the supernova rate per year (Condon & Yin 1990).[3] Andersen & Owen (1995) showed that radio sources in nearby clusters are offset from the radio–far-infrared relationship of field galaxies by typically a factor of two, and suggest that this is due to a boosting of the radio emission of cluster galaxies (for a given star-formation rate) due to compression of the magnetic field due to the motion of the galaxy through the intracluster medium; a more detailed study by Miller & Owen (2001) indicates that this applies only for a subsample of star-forming galaxies, is more prevalent in the richest clusters, and that the radio enhancement is typically a factor of 2 to 3. Based upon these results we include an extra factor of two into the above equation to account for this effect.

For a Salpeter initial-mass function with upper and lower mass cut-offs of 125 and 0.15 $M_\odot$, respectively, and assuming that all stars more massive than 8 $M_\odot$ produce supernovae, there is approximately one supernova for each 120 $M_\odot$ of star formation. Putting these together gives a relationship between the radio luminosity and the mean star-formation rate over the past ∼10^8 yr (the lifetime of the relativistic synchrotron electrons), $\dot{M}_*$, of:

$$\frac{\dot{M}_*}{{\rm M_\odot\,yr^{-1}}} \approx 4.5 \left(\frac{\rm GHz}{\nu}\right)^{-\alpha} \frac{L_\nu}{10^{22}\,{\rm W\,Hz^{-1}}}. \quad (1)$$

[3] For reference, the Milky Way has $n_{\rm SN} \simeq 0.041\,{\rm yr^{-1}}$ (Tammann 1982) and M82 has $n_{\rm SN} \simeq 0.1\,{\rm yr^{-1}}$ (Condon 1992).

In the following subsections this relation will be used to compare the radio source population with various other classes of cluster galaxies. In Subsection 5.1 the comparison between the cluster radio sources and the Butcher–Oemler population is considered. The correlation of the cluster radio sources with interacting and merging galaxies is investigated in Subsection 5.2, and the correlation with emission-line strengths is discussed in Subsection 5.3. The cluster radio source radio luminosity distribution is discussed in Subsection 5.4.

5.1 Correlations with galaxy colours

As discussed in the introduction, an increased proportion of bluer 'Butcher Oemler' galaxies, which are believed to have ongoing or recently terminated star formation, are found in high-redshift clusters. To investigate the radio emission from this 'Butcher Oemler' population in MS1054−03, the 10 cluster galaxies with colours bluer than $(U - B)_z = 0.1$ (excluding the blue Sc galaxy MS1054 − C5 which already lies within the radio source sample) were selected from the colour–magnitude diagrams of van Dokkum et al. (2000), and the mean radio emission from these was calculated. Only one of the galaxies was individually detected above the 2σ level, and that only at 2.1σ; the combined flux density from all ten galaxies was 2.4 ± 1.6 μJy, only a 1.5σ level detection. The measured mean radio flux density corresponds to $6 \pm 4\,{\rm M_\odot\,yr^{-1}}$, which is consistent with the star-formation rates necessary to bluen the galaxy colours by this amount. The current radio observations are not deep enough to detect typical star-forming galaxies, but only extreme starbursts or AGN activity.

Approaching this issue from the other side, in Fig. 4 is presented an F814W−F606W($\approx R - I$) versus F814W (I) colour–magnitude diagram for all of the early-type confirmed cluster galaxies, with the radio galaxies indicated as filled triangles, and the close pairs further indicated by a large circle. Excepting galaxy 5534 (one of the close pair of galaxies associated with MS1054−C3) all of the galaxies associated with the radio sources have colours consistent with the colour–magnitude relation of the other early types in the cluster. This suggests that their radio emission is not due to starburst activity, which would tend to bluen the galaxy colours, but rather with hidden AGN activity.

5.2 Correlations with galaxy–galaxy interactions

Of the eight cluster radio sources, four are associated with pairs of cluster galaxies with projected separations of 10–25 kpc (1–2.5 arcsec), that are plausibly undergoing interactions (although in the case of MS1054−C3 it must be noted that the velocity difference between the two galaxies in the pair is over 5000 km s^{-1}, and so this must either be a chance projection or, if an interaction, the galaxy pair is unbound; for MS1054−C6 although the second galaxy is not a spectroscopically-confirmed cluster member, its magnitude and colour are very strongly indicative that it is). The galaxies comprising these pairs are of type S0/a or earlier in seven of the eight cases, and are within one magnitude of each other in luminosity. The probability of a chance projection at these magnitudes and separations is ≪ 5 per cent, as discussed above.

Despite the apparent high proportion of 'interaction-driven' radio sources in the cluster, and the fact that the cluster is known to contain a very high proportion of confirmed binary galaxies and ongoing mergers (galaxy nuclei separated by ≪ 10 kpc), not a single one of the radio sources is associated with any of the 13 cluster objects classified 'merger/peculiar' by van Dokkum et al.

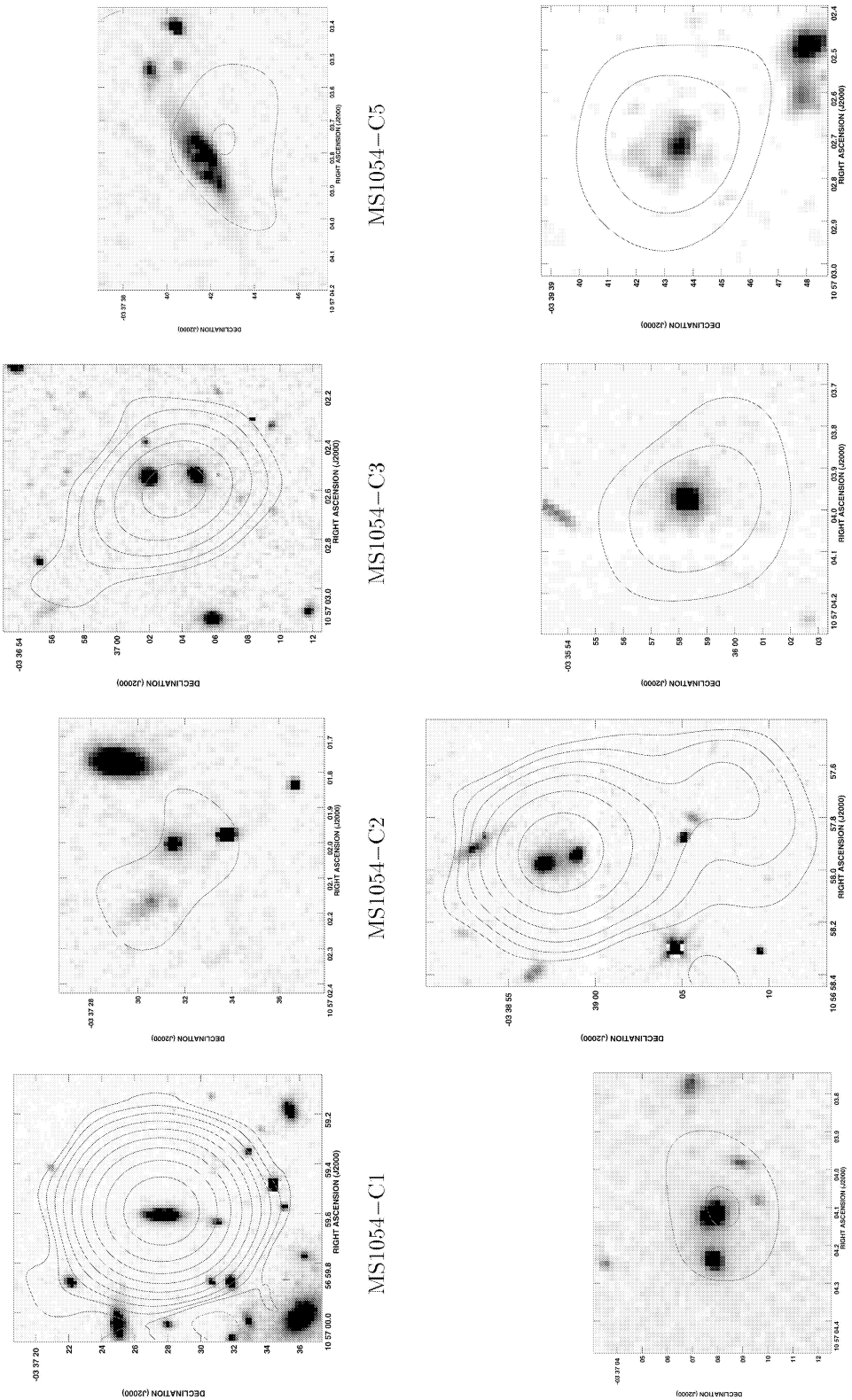

Figure 3. Radio contours of the eight radio sources confirmed to be associated with cluster galaxies, overlaid upon the optical images of their host galaxies. The radio contours are plotted at $(-2, -1, 1, 2, 4, 8, 16, 32, 64, 128, 256, 512) \times 16\,\mu\mathrm{Jy} > (3\sigma)$. The optical images are the F814W *HST* images, except for MS1054−C14 which lies outside of the *HST* field; for this source the *V*-band VLT image is displayed instead (see text for details). Note that in four out of the eight cases the radio emission is associated with one of a close pair of galaxies of similar magnitude.

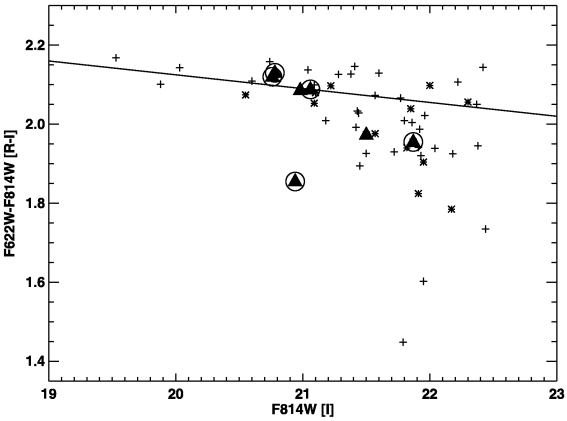

Figure 4. The F606W-F814W ($\approx R - I$) versus F814W colour–magnitude relation for the early-type galaxies in the MS1054 cluster. Crosses represent ellipticals and S0s, and asterisks are S0/a galaxies. Those galaxies associated with a radio source are indicated by filled triangles (in the case of close pairs, both of the pair of galaxies are indicated). The large circles indicate those radio galaxies that are one of a close pair. The line represents the fit to the colour–magnitude relation derived by van Dokkum et al. (2000). With only one exception, the galaxies associated with the radio sources have colours consistent with the tight colour–magnitude relation defined by the other early-type cluster galaxies.

(2000). Indeed, none of these merging galaxies is detected above the 2σ level in the radio map. This sets interesting limits on the radio luminosity associated with the cluster merger events: to provide tighter constraints, the radio emission was averaged across the locations of the 13 confirmed ongoing mergers in the cluster, giving a mean flux density of $2.2 \pm 1.5\,\mu$Jy, only a 1.5σ detection. Realistically then, the upper limit to the radio emission of the merger events is of order 5 μJy, which, at the redshift of the cluster, corresponds to a rest-frame 5-GHz radio luminosity of about $10^{22}\,\mathrm{W\,Hz^{-1}}$. From equation (1), this sets a limit on the mean of any starburst accompanying the merger events in the MS1054 cluster of order $10\,\mathrm{M_\odot\,yr^{-1}}$. This suggests that the very red colours generally seen for the merging galaxies (van Dokkum et al. 1999) are simply the intrinsic colours of the galaxies, rather than being caused by a massive starburst heavily obscured by dust.

The high proportion of galaxy pairs among radio sources in the cluster and the absence of radio emission from ongoing mergers implies that galaxy interactions may be more efficient than mergers at inducing radio activity. It is interesting to compare this result with that of Roche & Eales (2000) who found that the majority of a sample of powerful low-redshift 3CR radio galaxies were visibly interacting, but that the mean projected separation of the interacting pairs was 44 ± 10 kpc. This is about three times larger than that of interacting ultraluminous infrared galaxies. From this they concluded that radio bursts occurred at a much earlier stage of an interaction/merger than the peak of the starburst activity.

5.3 Correlations with emission-line luminosity

5.3.1 Line emission from star formation or AGN activity

In the absence of high-resolution radio observations or radio spectral indices to distinguish starbursting galaxies from AGNs, a separation between the two classes can still be made based upon the ratio of the radio to the emission-line luminosity of the host galaxies. When combined with optical morphologies and optical spectral properties, this division can be made with a fair degree of accuracy (e.g. Owen et al. 1999).

Very massive stars emit photons with high enough energy to ionize their surrounding gas, leading to a theoretical correlation (Barbaro & Poggianti 1997) between the [O II] 3727-Å emission-line luminosity and the mean star-formation rate over the past 10^7 yr (the approximate lifetime of such massive stars):

$$\frac{\dot{M}_*}{\mathrm{M_\odot\,yr^{-1}}} \approx 6.3\,\frac{L[\mathrm{O\,II}]}{10^{41}\,\mathrm{erg\,s^{-1}}}. \qquad (2)$$

In practice, however, use of the [O II] 3727-Å emission line as an estimator of star formation is fraught with problems (see, for example, Hopkins et al. 2001; Adelberger & Steidel 2000; Kennicutt 1998 and references therein), the most important of which is dust extinction, which causes the star-formation rate to be underestimated. These problems can, however, be mostly ignored if the level of accuracy required is only that to separate radio sources into starbursting galaxies or AGNs. The above conversion is therefore adopted, but with an allowance for optical extinction. Assuming that the average star-formation rate over the past 10^8 yr (sampled by the radio emission due to the synchrotron lifetime) is the same as that over the past 10^7 yr (sampled by the [O II] line emission), then equations (1) and (2) give a crude relationship between the observed 5-GHz radio flux density and the observed [O II] 3727-Å emission-line flux for a star-forming galaxy at redshift 0.83:

$$\frac{S_{5\,\mathrm{GHz}}}{\mu\mathrm{Jy}} \approx 4.4\,\frac{f[\mathrm{O\,II}]}{10^{-16}\,\mathrm{erg\,cm^{-2}\,s^{-1}}}\,\frac{1}{T_{[\mathrm{O\,II}]}}, \qquad (3)$$

where $T_{[\mathrm{O\,II}]}$ is the fraction of light transmitted (not extinguished) at 3727 Å. The scatter in both the line-luminosity-to-star-formation rate and radio-luminosity-to-star-formation rate relations, and the different star-formation timescales that the two relations sample, will provide further scatter around this relation.

No comparable relation is known between the [O II] 3727-Å and radio luminosities for AGNs at these radio luminosities, although the two properties are well correlated over several orders of magnitude, albeit with up to an order of magnitude of scatter, for more powerful radio galaxies (see fig. 3 of Willott et al. 1999); if this relation can be extrapolated down in luminosity then, converting the 151-MHz radio luminosity to a 5-GHz radio luminosity assuming a spectral index of 0.8:

$$\frac{S_{5\,\mathrm{GHz}}}{\mu\mathrm{Jy}} \approx 1.7\times10^4\left[\frac{f[\mathrm{O\,II}]}{10^{-16}\,\mathrm{erg\,cm^{-2}\,s^{-1}}}\right]^{1.45}. \qquad (4)$$

It is not clear whether such an extrapolation is valid; for example, Gruppioni, Mignoli & Zamorani (1999) find that a significant proportion of sub-mJy radio sources show only absorption lines and no emission lines. Irrespective of the precise details, however, the critical point is that for a given radio flux density the expected emission-line flux if the radio emission is produced by an AGN is at least 100–1000 times lower than if it is associated with star formation. A radio source with $S_{5\,\mathrm{GHz}} \sim 100\,\mu$Jy will only have detectable [O II] 3727-Å line emission if at least some of the radio emission is due to star formation.

5.3.2 The nature of the cluster radio sources

Only three of the eight cluster radio sources (MS1054−C1, C5, C14) are emission-line galaxies (defined as [O II] equivalent width

>5 Å; van Dokkum et al. 2000): MS1054−C1 has an [O II] 3727-Å equivalent width of 5.9 ± 1.2 Å; MS1054−C5 has 14.7 ± 2.2 Å; and MS1054−C14 has 39.0 ± 6.8 Å. Using the continuum magnitudes and colours from the *HST* observations to provide continuum calibration of the spectra, the [O II] 3727-Å fluxes of these three sources are compared with their radio fluxes in Fig. 5. The other five radio galaxies are similarly plotted, taking upper limits to the [O II] 3727-Å equivalent width of 5 Å. Also indicated on the figure is the relation for starburst galaxies derived in equation (3), with the shaded region representing the effect of up to two magnitudes of optical extinction. The extrapolated relation for AGN is also indicated, although once again it must be stressed that this relation is only indicative.

It is clear from Fig. 5 that MS1054−C1 is an AGN, as would be expected from its extreme radio luminosity. Equally, MS1054−C5 lies well within the region of the plot predicted for star-forming galaxies. Its radio flux density corresponds to a star-formation rate of nearly $100\,M_\odot\,yr^{-1}$; its morphology and colour are consistent with a high-current star-formation rate. MS1054−C14 lies between the AGN and starburst regions, and so the origin of its radio emission is less clear. This is likely either a heavily-extinguished starburst or a combination of AGN and star formation. The other five cluster galaxies all have upper limits to their emission-line luminosity that place them well below the star-formation region. The spectra of all five of these galaxies appear as typical elliptical galaxies. In two cases an extended radio source has been produced, so these must be AGNs; for the other three, although a heavily-obscured nuclear starburst cannot be excluded from these sources, similar low-luminosity radio sources in red ellipticals are found in low-redshift clusters and are seen to be weak AGNs (Owen et al. 1999). We conclude that these five sources are all likely to be weak AGNs.

Summarizing, of the four radio sources associated with isolated galaxies, two are AGNs, one is a starburst, and one is unclear. This is consistent with the 50–60 per cent starburst contribution at these luminosities, which has been both predicted on the basis of radio source count modelling (e.g. Wall & Jackson 1997; Hopkins et al. 2000) and observed in deep observations of the Hubble Deep Field (Richards et al. 1998). However, all four of the radio sources associated with galaxy pairs appear to be AGNs, and if confirmed then the overall AGN fraction amongst the cluster sources would be ≳75 per cent, inconsistent with field observations at these flux-density levels. The most likely explanation for this is that the isolated-cluster radio sources discussed above are essentially an extension of the field population, but that the galaxy pair radio sources represent a different population: interactions between early-type galaxies, inducing weak AGN activity, are unlikely to occur at a high rate in the field simply because of the sparsity of early types, and so this population may be fairly unique to high-redshift cluster environments.

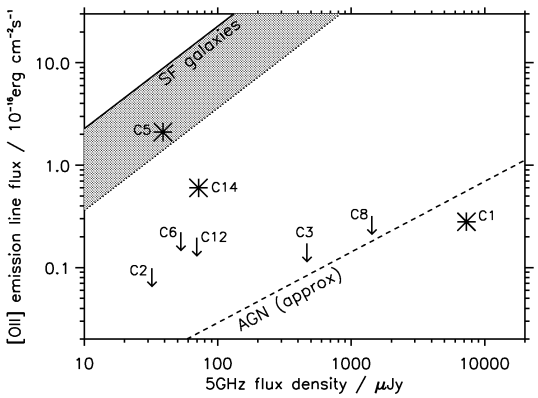

Figure 5. The distribution of [O II] 3727-Å line fluxes versus radio flux densities for the cluster radio sources. The relation expected for star-forming galaxies (Barbaro & Poggianti 1997) is indicated by the solid line, and the shaded region represents the effect of up to two magnitudes of dust extinction. The dashed line shows an extrapolation of the Willott et al. (1999) relation for powerful radio galaxies; its applicability at these lower radio luminosities is uncertain, but the key point is that the for a given radio luminosity, the emission-line luminosity is 2–3 orders of magnitude lower for AGNs than star-forming galaxies.

5.3.3 *Cluster emission-line galaxies*

None of the sources that van Dokkum et al. (2000) classified as emission-line galaxies (many of which also fall within the merger or blue galaxy categories) are detected above the 2σ level in the radio map apart from the three sources discussed above (C1, C5 and C14). The most emission-line luminous cluster galaxy, 1801, has $f([O\,II]) \approx 3\times10^{-16}\,erg\,cm^{-2}\,s^{-1}$, predicting a 15 μJy ($3\sigma$) radio flux density, although this is not detected in the radio maps. The mean radio emission of the emission-line galaxies, 0.9 ± 1.9 μJy, corresponds to an upper limit of about $5\,M_\odot\,yr^{-1}$, which is comparable with the mean star-formation rate of these galaxies determined using equation (2).

It is clear from these observations that radio surveys directly seek out both AGN and star-forming galaxies. A comparison with optical techniques demonstrates that at the current depth these observations are picking out the extreme end of the optically-selected star-forming galaxies together with a population of low-luminosity active galaxies that are not found using optical techniques. Still deeper observations will be required if typical star-forming galaxies are to be observed.

5.4 Cluster radio source luminosity distribution

Although the number of confirmed cluster radio sources in MS1054−03 is very small, it is still instructive to perform some simple comparisons with cluster radio populations at low redshift. Ledlow & Owen (1996) have determined the univariate and bivariate luminosity functions of radio sources in a sample of low-redshift ($z < 0.09$) clusters, from which can be determined the percentage of all elliptical galaxies brighter than absolute R-magnitude $M_R = -20.5$, which host radio sources more luminous than a given radio luminosity. For a galaxy with the colour of a typical early-type galaxy at $z = 0.83$, and taking into account also the R-magnitude change due to passive evolution of the stellar populations, this optical-magnitude limit corresponds to an apparent magnitude through the *HST* F814W filter of $I \sim 21.6$.

Within 1 Mpc (168 arcsec) of the centre of MS1054−03 there are 23 early-type galaxies (no separation is made here between ellipticals and S0 morphologies, and 3 of the 6 galaxies classified as 'S0/a', i.e. it is uncertain whether they are S0 or Sa, are included) with magnitudes $I < 21.6$ that are confirmed to be members of the cluster; the spectroscopic observations are currently over 80 per cent complete to this magnitude limit. Of these cluster early-type galaxies, 5 show radio emission with a rest-frame 1.4-GHz luminosity above $23.1\,W\,Hz^{-1}$ (again, including only 1 of the 2 S0/a classifications, and counting only one galaxy from each close pair). Given that the spectroscopic observations were taken prior to the radio observations, there is no reason to suspect that the

spectroscopic targets in any way favour those with radio emission, and hence the fraction 5/23 = 22 per cent should be a fair estimate of proportion of radio-loud early-type galaxies in the cluster. By comparison, Ledlow & Owen (1996) found that only 5.8 per cent of elliptical galaxies (and hence an even lower percentage of all early-type galaxies since very few of their S0s were radio emitting) in low-redshift clusters have radio luminosities above this level. Clearly there is an excess of radio sources in this high-redshift cluster compared with low-redshift clusters. However, this increase is only comparable with that found in the field: Hammer et al. (1995) found that the corresponding fraction for $z \gtrsim 0.7$ field ellipticals is of order one third.

Studying the Virgo cluster, Gavazzi & Boselli (1999) have shown that late-type galaxies of all Hubble types are equally likely to develop radio sources, with a probability proportional to the optical luminosity of the galaxy. Only two of the radio sources are unambiguously identified with late-type cluster galaxies (MS1054−C1 and C5), but it is instructive that these are indeed two of the most luminous late-type galaxies in the cluster (cf. van Dokkum et al. 2000).

As was discussed in the introduction, a deep radio survey of two $z \sim 0.25$ Abell clusters revealed a bimodality in the distribution of radio source luminosities in that cluster (see Fig. 6a), with the prevalence of the weaker radio source population providing a measure of the state of activity of the cluster (Dwarakanath & Owen 1999). Those galaxies classified as AGNs by Owen et al. (1999) have been shaded in the histogram: the more luminous radio source population is composed entirely of AGNs, whilst the weaker population provides a mixture of AGNs and starbursts. Smail et al. (1999) studied the cluster CL0939+4713 at $z = 0.41$, and their results are similarly plotted in Fig. 6b. In Fig. 6c is reproduced the histogram of radio luminosities of radio sources in the MS1054−03 cluster, converted from a 5- to a 1.4-GHz rest-frame assuming a spectral index of 0.8. The radio detection limit of each of the three clusters is indicated.

Whilst it cannot be over-stressed that these latter two clusters contain very small numbers of confirmed cluster galaxies, it is of note that both are consistent with the Abell 2125 distribution in the sense of being plausibly bimodal, with the more-luminous population consisting entirely of AGNs and the less-luminous population being both AGNs and starburst galaxies. Further, the break in luminosity between the two populations may evolve to higher luminosities as we move to higher redshifts: certainly the starburst galaxies detected in MS1054−03 are of higher radio luminosity than any detected in the low-redshift cluster. There are far too few cluster radio sources to attempt to quantify whether, and how quickly, any such evolution occurs. However, it is intriguing that the $(1+z)^{\approx 3}$ luminosity evolution, which matches the evolution of the luminosity functions of many different types of active galaxies (e.g. radio sources – Dunlop & Peacock 1993; optically-selected quasars – Maloney & Petrosian 1999; and X-ray sources – Boyle et al. 1993) fits the observations rather well.

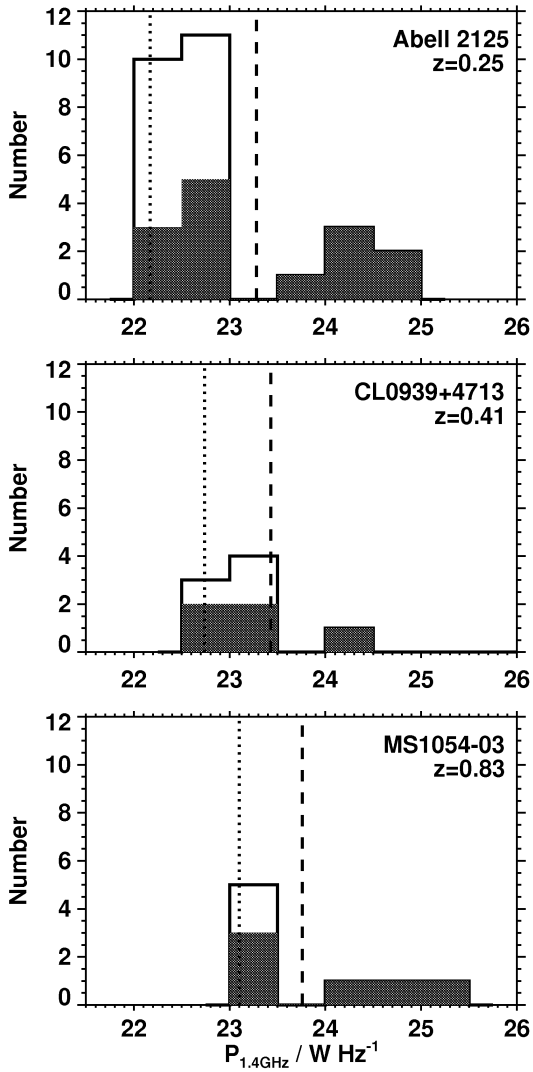

Figure 6. *Top:* the distribution of radio luminosities of radio sources associated with the $z = 0.25$ cluster Abell 2125. The data are from Dwarakanath & Owen (1999), converted to the cosmology assumed in this paper ($\Omega = 1$, $\Lambda = 0$, $H_0 = 70\,\mathrm{km\,s^{-1}\,Mpc^{-1}}$). The vertical dotted line represents the radio luminosity detection limit of the sample, and the dashed line indicates the centre of the break in the radio luminosity distribution. The shaded region indicates the AGN population, and the unshaded region comprises the starburst galaxies and unknown objects. The sources classified as AGNs by Owen et al. (1999) had either AGN spectra or were early-type galaxies with spectra showing no emission lines, thus inconsistent with being star-forming. *Middle:* the distribution of radio source luminosities in the cluster CL0939+4713 ($z = 0.41$) from Smail et al. (1999), again converted to the above cosmology. The dotted line is again the detection limit, and the dashed line shows the luminosity break derived for A2125, scaled up in luminosity according to $(1+z)^3$ evolution. The AGN galaxies are similarly defined. *Bottom:* the distribution of radio luminosities of sources whose host galaxies are confirmed to be associated with MS1054−03 at $z = 0.83$; the MS1054−03 data has been converted to a 1.4-GHz rest-frame luminosity assuming a spectral index of 0.8. The two vertical lines are as defined for CL0939+4713.

6 CONCLUSIONS

Deep radio imaging of the $z = 0.83$ cluster MS1054−03 has revealed a population of cluster radio sources. Eight radio sources are associated with galaxies that are already spectroscopically-confirmed cluster members. This corresponds to approximately 22 per cent of early-type confirmed cluster galaxies with $M_R < -20.5$ within 1 Mpc of the cluster centre having rest-frame 1.4-GHz luminosity above 23.1 W Hz^{-1}. The cluster radio sources fall into two distinct categories. Four sources are hosted by isolated galaxies that have a range of morphologies from ellipticals to Sc galaxies; the radio emission appears to be associated with a starburst in at least one case, and AGN activity in two. The other four cluster radio sources are associated with close pairs of

galaxies, possibly interacting, although not all bound systems. Seven of the eight galaxies comprising these pairs are of type S0/a or earlier, and the radio emission from these galaxy pairs is almost certainly nuclear in origin. This $\gtrsim 75$ per cent proportion of AGNs in the cluster is in contrast to the field, where $\sim 50-60$ per cent of radio sources at this flux-density level are associated with starburst galaxies. Considering the isolated-cluster radio galaxies alone, these are consistent with the field distribution and may essentially be an extension of it, with the radio sources associated with galaxy pairs being a new AGN population, driven by early-type galaxy interactions, and thus fairly unique to high-redshift cluster environments.

MS1054−03 is a cluster that contains a high proportion of ongoing mergers. However, although up to 50 per cent of the confirmed cluster radio sources appear to be interaction driven, none is associated with the confirmed merger events, and the upper limit to the mean radio luminosity of these merger events is of order $10^{22}\,\mathrm{W\,Hz^{-1}}$, comparable with that of M82. It appears that galaxy–galaxy interactions may be more efficient than direct mergers at inducing radio emission.

Although the sample of confirmed cluster radio sources is small (eight), the cluster radio luminosity function shows a hint of bimodality, mirroring that observed in the low-redshift cluster Abell 2125, with a possible increase in the break luminosity with redshift.

Clearly, to investigate these issues further, spectroscopic redshifts for the remainder of the radio sources in the sample will be required, together with deep radio surveys of a larger sample of distant clusters to improve the statistics and confirm the results suggested here.

ACKNOWLEDGMENTS

The National Radio Astronomy Observatory is operated by Associated Universities Inc., under co-operative agreement with the National Science Foundation. PNB would like to thank the Royal Society for generous financial support through its University Research Fellowship scheme. PGvD acknowledges support by NASA through Hubble Fellowship Grant HF-01126.01-99A awarded by the Space Telescope Science Institute, which is operated by the Association of Universities for Research in Astronomy, Inc., for NASA under contract NAS 5-26555. We thank the anonymous referees for useful comments.

REFERENCES

Adelberger K. L., Steidel C. C., 2000, ApJ, 544, 218
Andersen V., Owen F. N., 1995, AJ, 109, 1582
Baars J. W. M., Genzel R., Pauliny-Toth I. I. K., Witzel A., 1977, A&A, 61, 99
Barbaro G., Poggianti B. M., 1997, A&A, 324, 490
Bertin E., Arnouts S., 1996, A&A Supp., 117, 393
Boyle B. J., Griffiths R. E., Shanks T., Stewart G. C., Georgantopoulos I., 1993, MNRAS, 260, 49
Butcher H. R., Oemler A., 1978, ApJ, 219, 18
Condon J. J., 1992, ARA&A, 30, 575
Condon J. J., Yin Q. F., 1990, ApJ, 357, 97
Djorgovski S., Davies M., 1987, ApJ, 313, 59
Donahue M., Voit G. M., Gioia I., Lupino G., Hughes J. P., Stocke J. T., 1998, ApJ, 502, 550
Donnelly R. H., Partridge R. B., Windhorst R. A., 1987, ApJ, 321, 94
Dressler A., 1984, ARA&A, 22, 185
Dressler A., Lyndon-Bell D., Burstein D., Davies R. L., Faber S. M., Terlevich R., Wegner G., 1987, ApJ, 313, 42
Dressler A. et al., 1997, ApJ, 490, 577
Dressler A., Smail I., Poggianti B. M., Butcher H., Couch W. J., Ellis R. S., Oemler A., 1999, ApJ, Supp., 122, 51
Dunlop J. S., Peacock J., 1993, MNRAS, 263, 936
Dwarakanath K. S., Owen F. N., 1999, ApJ, 118, 625
Fanaroff B. L., Riley J. M., 1974, MNRAS, 167, 31
Fomalont E. B., Windhorst R. A., Kristian J. A., Kellerman K. I., 1991, AJ, 102, 1258
Garrett M. A., de Bruyn A. G., Giroletti M., Baan W. A., Schilizzi R. T., 2000, A&A, 361, 41
Gavazzi G., Boselli A., 1999, A&A, 343, 86
Gioia I. M., Maccacaro T., Schild R. E., Wolter A., Stocke J. T., Morris S. L., Henry J. P., 1990, ApJ, Suppl., 72, 567
Giovannini G., Tordi M., Feretti L., 1999, New Astronomy, 4, 141
Gruppioni C., Mignoli M., Zamorani G., 1999, MNRAS, 304, 199
Gunn J. E., Gott J. R., 1972, ApJ, 176, 1
Haarsma D. B., Partridge R. B., Windhorst R. A., Richards E. A., 2001, ApJ, 544, 641
Hammer F., Crampton D., Lilly S. J., Le Fèvre O., Kenet T., 1995, MNRAS, 276, 1085
Hopkins A., Windhorst R., Cram L., Ekers R., 2000, Experimental Astronomy, 10, 419
Hopkins A., Connolly A., Haarsma D., Cram L., 2001, AJ, 122, 288
Jeltema T. E., Canizares C. R., Bautz M. W., Malm M. R., Donahue M., Garmire G. P., 2001, ApJ, in press (astro-ph/0107314)
Kennicutt R. C., 1998, ARA&A, 36, 189
Ledlow M. J., Owen F. N., 1996, AJ, 112, 9
Madau P., Pozzetti L., Dickinson M., 1998, ApJ, 498, 106
Maloney A., Petrosian V., 1999, ApJ, 518, 32
Miller N. A., Owen F. N., 2001, AJ, 121, 1903
Muxlow T. W. B., Wilkinson P. N., Richards A. M. S., Kellerman K. I., Richards E. A., Garrett M. A., 1999, New Astron. Rev., 43, 623
Owen F. N., Ledlow M. J., Keel W. C., Morrison G. E., 1999, AJ, 118, 633
Pascarelle S. M., Lanzetta K. M., Fernández-Soto A., 1998, ApJ, 508, L1
Poggianti B. M., Smail I., Dressler A., Couch W. J., Barger A. J., Butcher H., Ellis R. S., Oemler A., 2000, ApJ, 518, 576
Richards E. A., Kellermann K. I., Formalont E. B., Windhorst R. A., Partridge R. B., 1998, AJ, 116, 1039
Roche N., Eales S. A., 2000, MNRAS, 317, 120
Schade D., Barrientos L. F., Lopez-Cruz O., 1997, ApJ, 477, L17
Smail I., Morrison G., Gray M. E., Owen F. N., Ivison R. J., Kneib J.-P., Ellis R. S., 1999, ApJ, 525, 609
Stanford S. A., Eisenhardt P. R., Dickinson M., 1998, ApJ, 492, 461
Stocke J. T., Perlman E. S., Gioia I. M., Harvanek M., 1999, AJ, 117, 1967
Tammann G. A., 1982, in Rees M. J., Stoneham R. J., eds, Supernovae: a Survey of Current Research. Reidel, Dordrecht, p. 371
van Dokkum P. G., Franx M., Kelson D. D., Illingworth G. D., 1998a, ApJ, 504, L17
van Dokkum P. G., Franx M., Kelson D. D., Illingworth G. D., Fisher D., Fabricant D., 1998b, ApJ, 500, 714
van Dokkum P. G., Franx M., Fabricant D., Kelson D. D., Illingworth G. D., 1999, ApJ, 520, L95
van Dokkum P. G., Franx M., Fabricant D., Illingworth G. D., Kelson D. D., 2000, ApJ, 541, 95
Wall J. V., Jackson C. A., 1997, MNRAS, 290, L22
Willott C. J., Rawlings S., m. Blundell K., Lacy M., 1999, MNRAS, 309, 1017
Windhorst R. A., van Heerde G., Katgert P., 1984, A&A Supp., 58, 1
Windhorst R. A., Miley G. K., Owen F. N., Kron R. G., Koo D. C., 1985, ApJ, 289, 494
Windhorst R. A., Formalont E. B., Partridge R. B., Lowenthal J. D., 1993, ApJ, 405, 498
Windhorst R. A., Formalont E. B., Kellermann K. I., Partridge R. B., Richards E., Franklin B. E., Pascarelle S. M., Griffiths R. E., 1995, Nat, 375, 471

APPENDIX A: THE INDIVIDUAL SOURCES

In this appendix the nature of each individual source is discussed, ordered by radial distance from the centre of the cluster, and radio-contour maps of the field of each source are displayed in Fig. A1. For those radio sources that lie within sky area of the *HST* mosaic, the radio sources are shown overlaid upon a grey-scale representation of the F814W (I) image. In each case the grey-scale range is exactly the same, so the relative brightness of the objects can be compared with that of the brightest cluster galaxy, visible in the MS1054−C1 field. Those radio sources that lie outside of the *HST* mosaic but within the larger field of the FORS imaging are shown overlaid upon the V-band image, the grey-scale range of the latter being adjusted to be at levels comparable with that of the F814W image grey-scales. The remaining nine sources that lie outside the FORS fields are simply displayed as radio-contour plots.

Details of the individual sources are as follows.

MS1054−C1: First detected in the shallower imaging of Stocke et al. (1999), this bright radio source is associated with a confirmed cluster Sc galaxy. This galaxy is projected close to the cluster centre (the elliptical galaxy visible 6.4 arcsec east and 8.3 arcsec south of this galaxy is the central cluster galaxy) although offset in velocity by over 2000 km s^{-1}. Its high radio luminosity (1.3×10^{25} W Hz^{-1}) indicates that the radio emission must be associated with AGN activity, and the radio-to-emission-line flux-density ratio confirms this (Fig. 5).

MS1054−C2: The most tenuous radio detection in the sample, this radio emission arises from the vicinity of three optically-detected galaxies, two of which are confirmed cluster members projected less than 20 kpc apart, and the third of which lies at higher redshift ($z = 1.076$). It is unclear whether the emission is associated with just one of the galaxies, or with more, perhaps from a combination of two cluster galaxies due to an interaction.

MS1054−C3: This relatively bright radio source was also detected in the shallower observations of Stocke et al. (1999). It lies between two confirmed cluster galaxies, not especially consistent with the location of either (though note that the position determined by Stocke et al. places it closer to the southern galaxy). The two galaxies may be interacting, separated by a projected distance of only 17 kpc, although the colours of both galaxies are red: one galaxy lies on the 'passive-evolution' colour–magnitude relation and the other is about 0.2 mag bluer than this (Fig. 4). The radio source is extended by the order of the separation of the two galaxies, and shows a marginal detection of polarization (see Fig. A2), indicating that the radio emission is likely to have an AGN origin.

MS1054−C4: This extended region of radio emission has no obvious optical counterpart in the deep *HST* images. Its nature is unclear, although its luminosity and radial offset from the cluster centre are both consistent with its being a cluster relic radio source: these are diffuse radio sources found occasionally in clusters, associated with no particular parent galaxy (e.g. Giovannini, Tordi & Feretti 1999 and references therein). Their origin is still uncertain.

MS1054−C5: This region of weak radio emission appears to be separate from the extended source MS1054−C4, although it cannot be ruled out that these form part of the same source. Far more likely is that this emission is associated with starbursting activity in the $z = 0.8113$ cluster Sc galaxy projected only 1.2 arcsec away: as shown in Section 5.3, the radio luminosity of the source is very close to that which would be predicted on the basis of the emission-line luminosity of this Sc galaxy, assuming both to be associated with ongoing star formation.

MS1054−C6: This radio emission is associated with a confirmed cluster elliptical galaxy, whose isophotes overlap with a second elliptical galaxy of comparable magnitude and colour (but unknown redshift). Other fainter galaxies are observed close-by. If the second elliptical galaxy is also a cluster member, then the radio emission is likely to have been induced by galaxy–galaxy interaction.

MS1054−C7: Although there is a small possibility that this radio emission forms part of the extended radio source MS1054 − C8, it appears to be a separate radio source associated with a 22nd-magnitude galaxy, whose redshift is currently unknown.

MS1054−C8: This bright radio source was first detected by Stocke et al. (1999) and is associated with two galaxies both of which are confirmed cluster members with a projected separation of 11 kpc. These galaxies may be interacting, but do not show any features that would cause them to have been classified as a merger by van Dokkum et al. (1999). The extended structure of this AGN is consistent with a core–jet source. A core-dominated (i.e. beamed) quasar is unlikely since neither of the associated galaxies has magnitudes or colours indicating a strong nuclear component.

MS1054−C9: This unresolved weak radio source has no obvious optical identification on the deep *HST* mosaic, although the location of the source, on the diffraction spike of a nearby 19th-magnitude star, may have precluded any faint optical galaxy from being identified on the *HST* image. This star provides the entry in Table 3, but is unlikely be the true radio source host given the radio–optical offset.

MS1054−C10: A pair of very faint ($I \sim 23.5$) blue galaxies is seen at the location of this radio source, although redshifts are not available for either of them.

MS1054−C11: The 23rd-magnitude galaxy that lies within half an arcsec of the position of this weak radio source has no measured redshift.

MS1054−C12: This unresolved radio source is unambiguously identified with an early-type galaxy at the redshift of the cluster.

MS1054−C13: This radio source corresponds to a 22nd-magnitude Sab galaxy of unknown redshift. The brighter galaxy a few arcsec to the north-east of the radio source has a redshift of $z = 0.17$, and is unlikely to be related.

MS1054−C14: This radio source is associated with a diffuse optical galaxy at the cluster redshift.

MS1054 − C15: This weak extended radio emission appears to be associated with a bright spiral galaxy at redshift 0.25. The measured flux density corresponds to a radio luminosity of 1.2×10^{22} W Hz^{-1}, similar to that of M82.

MS1054−C16: No optical counterpart brighter than $I \approx 26$ is seen associated with this unresolved radio source.

MS1054−C17: At the location of this radio source there is only a marginal detection of an extremely faint galaxy ($I \sim 26$).

MS1054−C18: This luminous extended radio source, which has an edge-darkened structure compatible with being an FR I type source (Fanaroff & Riley 1974) is associated with a low-redshift ($z = 0.182$) elliptical galaxy that has a second galaxy projected 3 arcsec away to the NNE (within the saturated region of the presented grey-scale), almost certainly undergoing an interaction. The radio source is quite strongly polarized (see Fig. A2) with a well-ordered polarization structure along the source axis in the central regions but perpendicular to this at the extremities.

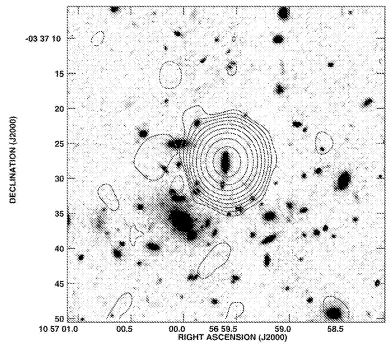

MS1054−C1

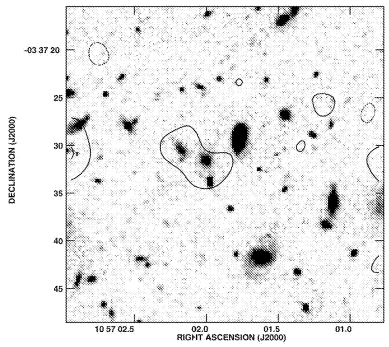

MS1054−C2

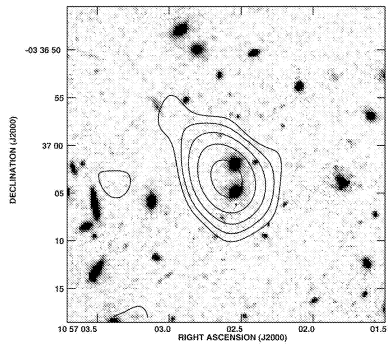

MS1054−C3

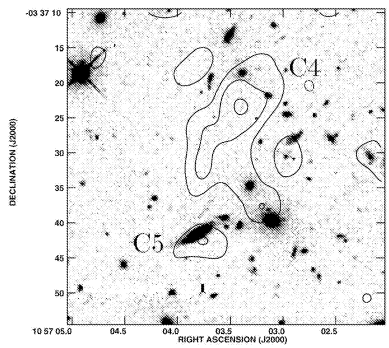

MS1054−C4 & C5

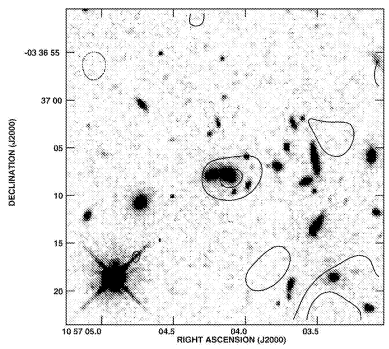

MS1054−C6

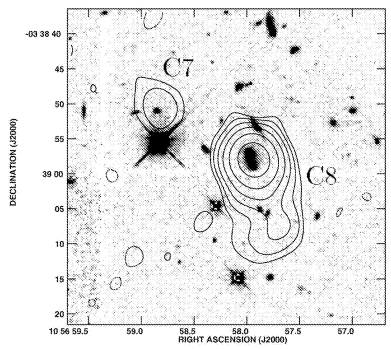

MS1054−C7 & C8

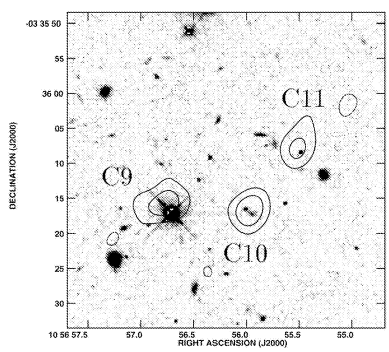

MS1054−C9, C10 & C11

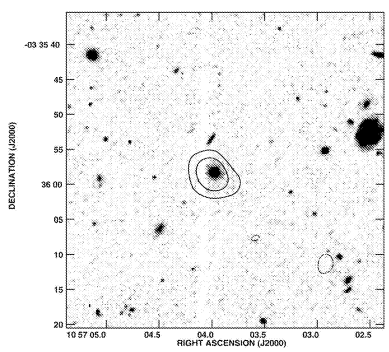

MS1054−C12

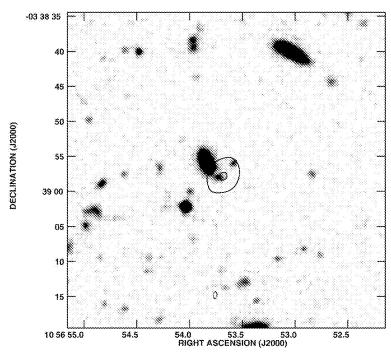

MS1054−C13

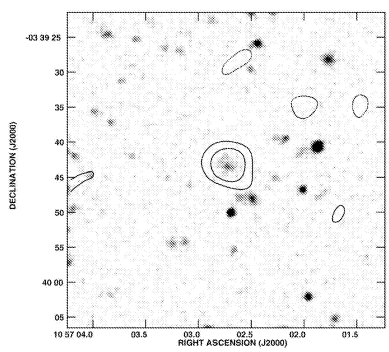

MS1054−C14

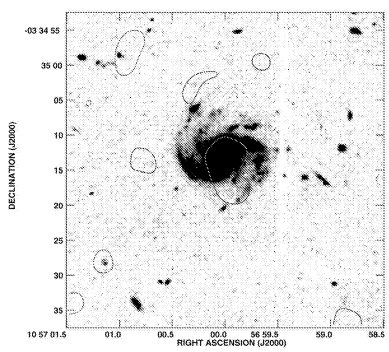

MS1054−C15

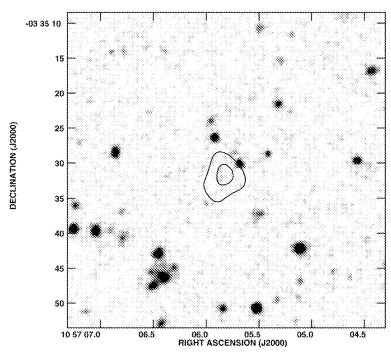

MS1054−C16

Figure A1. Contour plots of the 34 radio sources detected within 400 arcsec of the centre of the MS1054−03 cluster. Note that in some cases, where the radio sources are projected close together, more than one radio source is present in the plot. This is indicated by the labelling on and underneath each figure. The contours are plotted at $(-2, -1, 1, 2, 4, 8, 16, 32, 64, 128, 256, 512) \times 16\,\mu$Jy ($3\sigma$), except for MS1054−C34, where the contours at 8.0 μJy (1.5σ) have also been added better to display the extended structure, and MS1054−C4+5, where the first contour level was 13 μJy (2.5σ) to provide a clearer figure. Overlaid

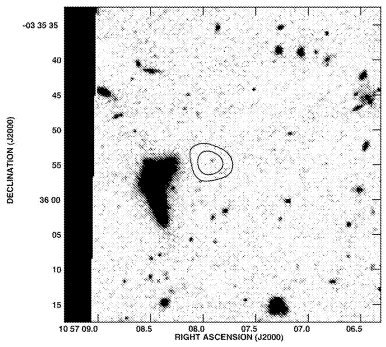

MS1054−C17

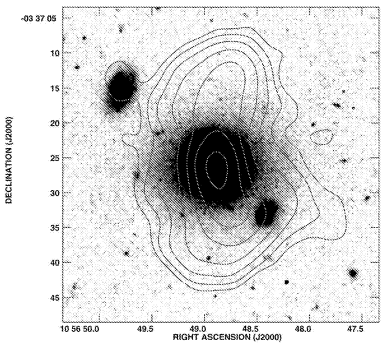

MS1054−C18

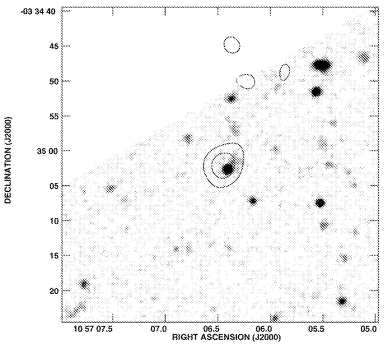

MS1054−C19

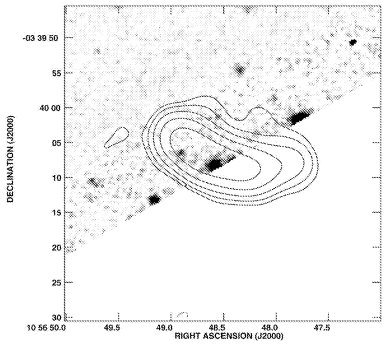

MS1054−C20

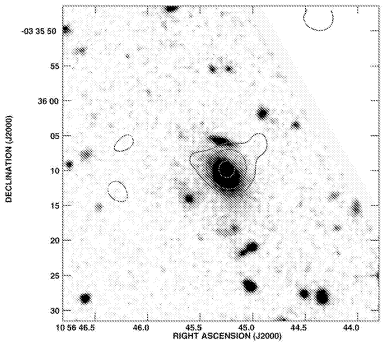

MS1054−C21

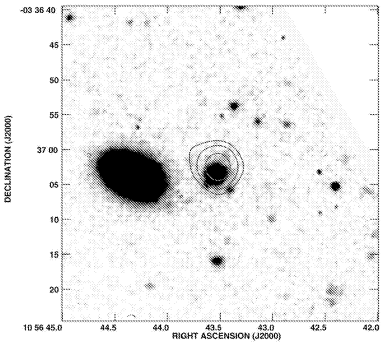

MS1054−C22

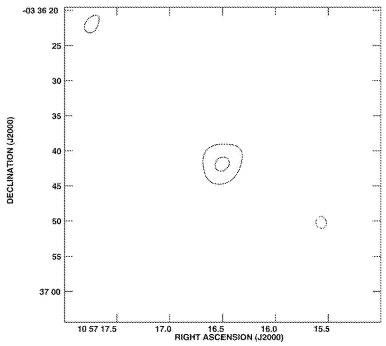

MS1054−C23

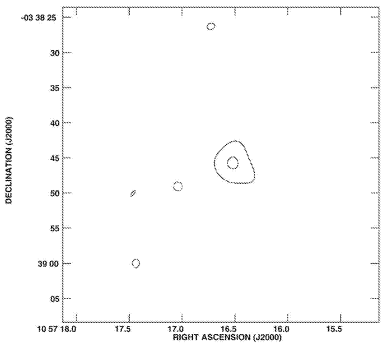

MS1054−C24

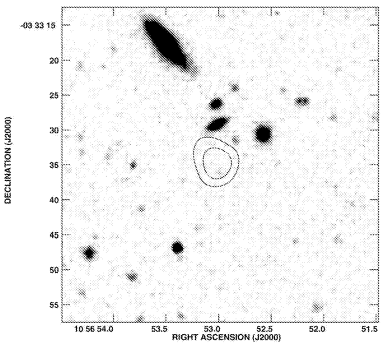

MS1054−C25

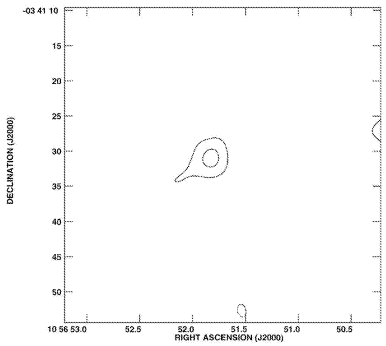

MS1054−C26

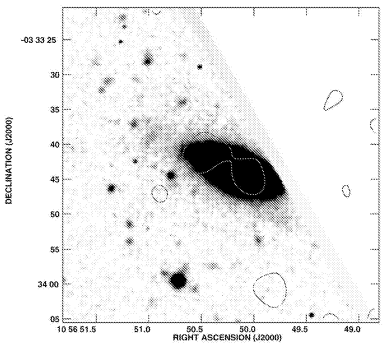

MS1054−C27

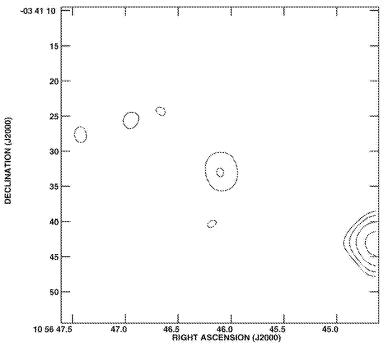

MS1054−C28

upon these contour plots for the radio sources MS1054−C1, C2, C3, C4 & C5, C6, C7 & C8, C9 & C10 & C11, C12, C15, C17 and C18 are grey-scale images taken through the F814W (*I*) filter of the *HST*; grey-scale *V*-band images taken with FORS on the VLT are overlaid for radio sources MS1054−C13, C14, C16, C19, C20, C21 C22, C25, C27 and C29. Within each group (i.e. the F814W and the *V*-band images) the grey-scale-intensity range is held constant, and has been adjusted to be comparable between the two groups. Thus the brightness of the host radio galaxies can be visually compared with that of the brightest cluster galaxy, which is the elliptical galaxy visible in the field of MS1054−C1 at position 10 57 00.02, −3 37 36.0.

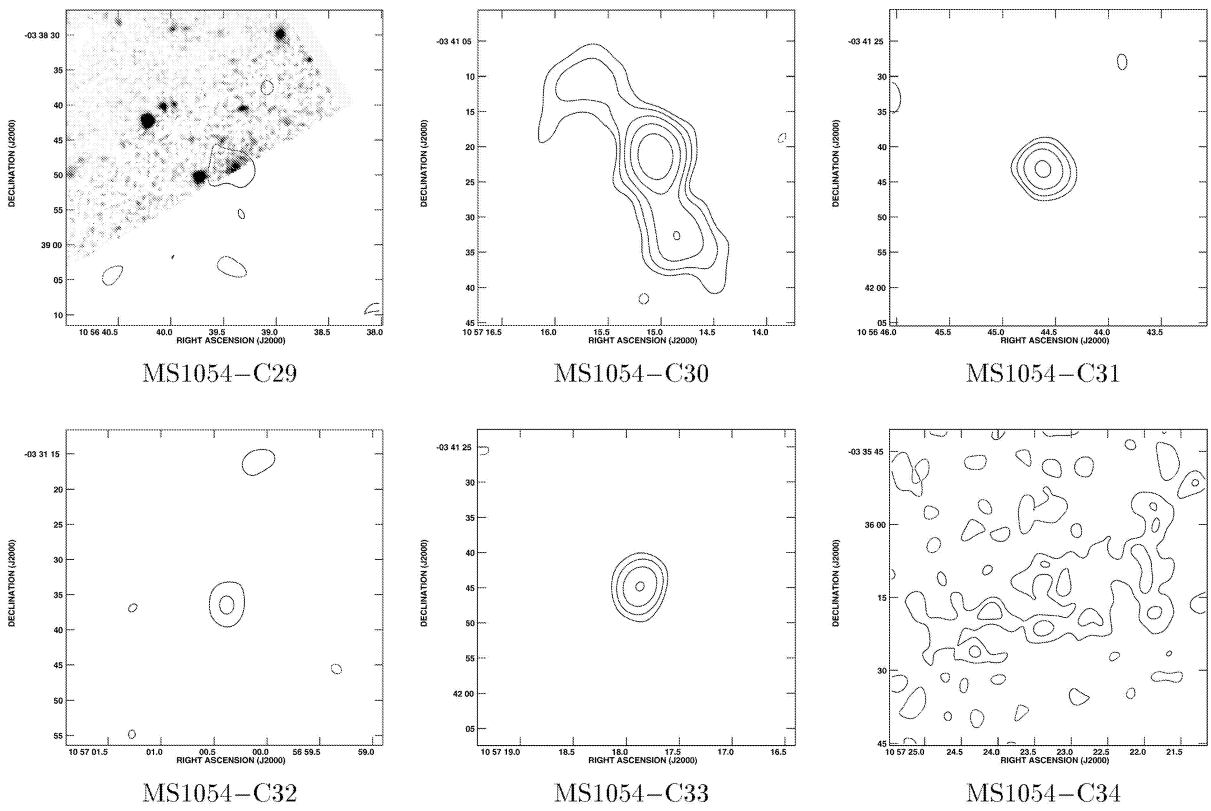

Figure A1. – *continued*

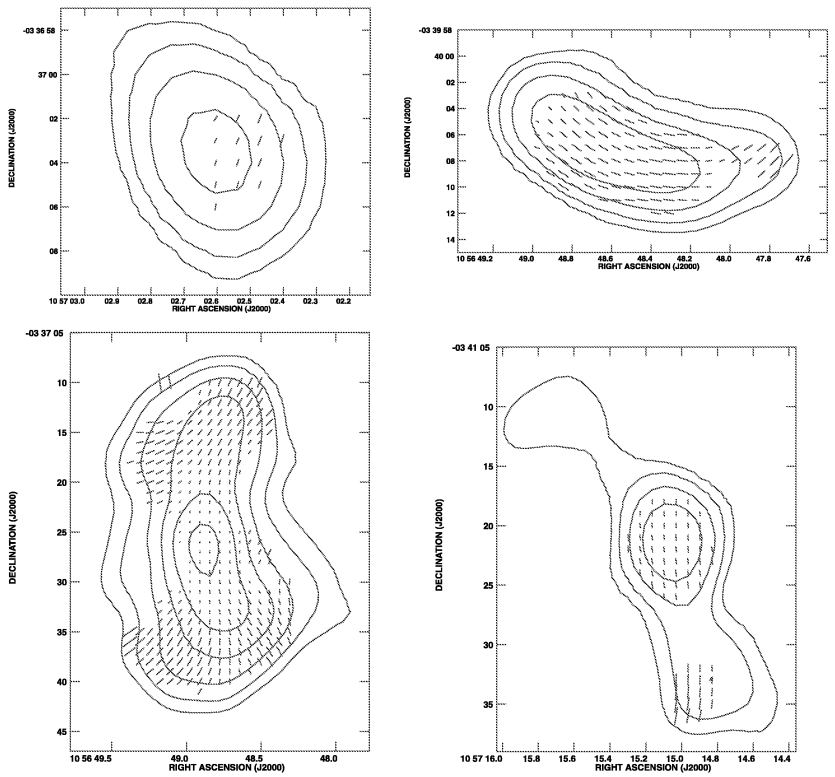

Figure A2. Contour plots with electric polarization vectors overlaid for the four radio sources that show polarized emission. The contours are at $(-1,\ 1,\ 2,\ 4,\ 8,\ 16,\ 32,\ 64) \times 32\,\mu\mathrm{Jy\,beam^{-1}}$, and a polarization vector of length 1 arcsec corresponds to 50 per cent polarization. The sources are: upper left – MS1054−C3; lower left – MS1054−C18; upper right – MS1054−C20; lower right – MS1054−C30.

MS1054−C19: An optical galaxy lies within half an arcsec of the position of this possibly-resolved radio source, but its redshift is unknown.

MS1054−C20: This extended source could have either FR I or head–tail structure and shows strong polarization throughout, parallel to the extended radio structure (Fig. A2). It lies at the very edge of the optical frame, but appears to have an associated optical counterpart.

MS1054−C21: A galaxy at redshift $z = 0.374$ lies roughly coincident with this weak unresolved radio source. The corresponding rest-frame 5 GHz radio luminosity is 4×10^{22} W Hz^{-1}, consistent with the radio emission being associated with star-formation activity.

MS1054−C22: This unresolved radio source has a relatively unambiguous optical counterpart that has not been observed spectroscopically.

MS1054−C23: This unresolved radio source lies outside the field of the optical images.

MS1054−C24: This unresolved radio source lies outside the field of the optical images.

MS1054−C25: No optical counterpart is seen at the location of this radio source.

MS1054−C26: This unresolved radio source lies outside the field of the optical images.

MS1054−C27: A low-redshift spiral galaxy is clearly the source of this extended radio emission. Although the galaxy has not been observed spectroscopically, its bright magnitude suggests a low redshift, implying that the radio emission is likely to be associated with ongoing star formation.

MS1054−C28: This unresolved radio source lies outside the field of the optical images.

MS1054−C29: This radio source is possibly resolved and lies at the very edge of the optical image. An optical galaxy partially seen at the edge of the image appears to be associated with it.

MS1054−C30: Extending nearly half an arcmin on the sky, this radio source is clearly brightest at its centre and probably has FR I structure, although an FR II structure with a bright radio core cannot be excluded. The central radio region is highly polarized, with the electric field vectors lying parallel to the extended radio structure. The radio source lies outside the field of the optical images.

MS1054−C31: This unresolved radio source lies outside the field of the optical images.

MS1054−C32: This unresolved radio source lies outside the field of the optical images.

MS1054−C33: This unresolved radio source lies outside the field of the optical images.

MS1054−C34: A large diffuse area of radio emission, extending an arcmin or more, is detected at this location. It lies outside of the optical frames, and no luminous nearby galaxies are seen in the digitized sky catalogues at this location, so its nature remains unclear. One possibility again is that this is associated with a cluster relic radio source; although it is found much further from the centre of the cluster (2.2 Mpc) than is typical for these sources, such large-radii relics have been observed before (e.g. in Abell 2345; Giovannini et al. 1999).

This paper has been typeset from a TEX/LATEX file prepared by the author.